Ventral dentate gyrus-dominated LFP rhythmicity in the social brain reflects the context of social encounters

Alok Nath Mohapatra[1], David Peles[1], Shai Netser[1], Shlomo Wagner[1,*]

[1] Sagol Department of Neurobiology, Faculty of Natural Sciences, University of Haifa, Haifa, Israel

*Corresponding author: shlomow@research.haifa.ac.il

Corresponding author: Shlomo Wagner, Sagol Department of Neurobiology, the Integrated Brain and Behavior Research Center (IBBRC), Faculty of Natural Sciences, University of Haifa, Mt. Carmel, Haifa 3498838, Israel.

Tel.: (972)-4-8288773, Fax: (972)-4-8288763, Email: shlomow@research.haifa.ac.il

Abstract

Mammalian social behavior is highly context-sensitive. Yet, nothing is known about the mechanisms that modulate social behavior according to its context. Recent studies have revealed a network of mostly limbic brain regions, here termed the "social brain", which regulates social behavior. We hypothesized that coherent theta and gamma rhythms couple regions of the social brain into functional networks in a context-dependent manner. To test this concept, we simultaneously recorded extracellular activity from multiple social brain regions in mice performing three social discrimination tasks. Local field potential rhythmicity during a task was mainly sensitive to an internal arousal state. However, during stimulus investigation we observed a distinct state, which was sensitive to stimulus characteristics. Yet, the coherence between the various regions was most sensitive to the social context. Moreover, we found the ventral dentate gyrus to play a pivotal role in coordinating the context-specific rhythmic activity in the network.

Brain-region name abbreviations

AcbC: Accumbens nucleus, core
AcbSh: Accumbens nucleus, shell
AhiAL: Amygdalo-hippocampal area, anterolateral part
BLA: Basolateral amygdaloid nucleus
BMP: Basomedial amygdaloid nucleus, posterior part
DMD: Dorsomedial hypothalamic nucleus, dorsal part
EA: Extended amygdala
IL: Infralimbic prefrontal cortex
LS: Lateral septum
MeAD: Medial amygdaloid nucleus, anterodorsal
Pir: Piriform cortex
PLH: Peduncular part of the lateral hypothalamus
PrL: Prelimbic prefrontal cortex
PVN: Paraventricular hypothalamic nucleus
vCA1: Field CA1 of the hippocampus, ventral part
vDG: Dentate gyrus, ventral part
VP: Ventral pallidum

Introduction

Mammalian social behavior is highly complex and dynamic, involving multiple types of distinct, sometimes even opposing, interactions between partners. Indeed, the identity of a partner can completely change the nature and trajectory of social actions taken by an individual (Adolphs, 2010). In addition to these complexities, social interactions are highly dependent upon the social context. For example, humans will most likely respond differently to a hand placed upon their shoulder from behind if this happens in a frightening context, such as in a dark alley in a foreign city, than if the same contact occurs in a cocktail party. Presently, little is known of the brain mechanisms and neural circuits that encode the context of social encounters and change responses to social cues accordingly.

In the last two decades, studies have begun to reveal the brain circuits that sub-serve various types of social behavior (for recent review papers see for example Ford and Young, 2021; Kohl and Dulac, 2018; McKinsey et al., 2018; Wei et al., 2021). Such studies exposed the involvement of a vast network of mostly sub-cortical limbic brain regions, here termed the "social brain" (Insel and Fernald, 2004), in processing social sensory cues and regulating mammalian social behavior (Dickinson et al., 2022; Goodson, 2005). These include striatal regions, such as the nucleus accumbens core (AcbC) and shell (AcbSh), the prelimbic (PrL) and infralimbic (IL) prefrontal cortical areas, several hippocampal and septal areas and multiple amygdaloid and hypothalamic nuclei (Dai et al., 2022; Felix-Ortiz and Tye, 2014; Kingsbury et al., 2020; Leroy et al., 2018). Many of these areas are highly interconnected in a bidirectional manner (Kohl et al., 2018; Scheggia et al., 2022; Swanson et al., 2020; Twining et al., 2017; Yamamoto et al., 2018), and some were shown to be involved in various, at times opposing, types of social behavior (Dai et al., 2022; Dolen et al., 2013; Felix-Ortiz et al., 2016; Huang et al., 2020; Reis et al., 2021). It remains, however, unclear how this intricate network of brain areas generates the large repertoire of distinct types of social behavior. Recent studies using multi-site brain recordings from behaving animals have demonstrated that system-level neural activity in sub-networks of the social brain predict individual social preferences (Mague et al., 2022) and decision-making (Schaich Borg et al., 2017) better than does local neural activity at any single brain region. These results thus suggest that coding of the various aspects of social behavior in the brain should be considered at the system level.

Oscillatory neural activity, mostly in the theta (4-12 Hz) and gamma (30-80 Hz) bands, was reported in many cortical and sub-cortical brain regions in various species (Buzsaki and Draguhn, 2004; Harris and Gordon, 2015a; Uhlhaas et al., 2009), with its power being shown to intensify during demanding cognitive functions, such as learning (Bocchio et al., 2017; Chen et al., 2021; Taub et al., 2018) and social communication (John et al., 2022; Kuga et al., 2022; Tendler and Wagner, 2015). Furthermore, abnormal

68 theta and gamma rhythms have been reported in multiple neurodevelopmental disorders (Buzsaki and
69 Watson, 2012; Cannon et al., 2014; Uhlhaas et al., 2010), such as autism spectrum disorder (ASD)
70 (Geschwind and Levitt, 2007; Lazaro et al., 2019). Accordingly, one prominent hypothesis states that
71 coherent manifestation of these rhythms can dynamically coordinate the activity of neural ensembles
72 dispersed over multiple brain regions and link them into *ad hoc* functional networks (Fries, 2015).
73 In the present study, we hypothesized that coherent theta and gamma rhythms couple various regions of
74 the social brain into functional networks in a social context-dependent manner. In other words, distinct
75 social contexts dictate different patterns of coordinated rhythmic activity of dispersed social brain
76 neuronal ensembles, which in turn subserve context-dependent processing of social cues and consequent
77 behavioral responses. To test this hypothesis, we recorded extracellular electrical activity simultaneously
78 from multiple regions of the social brain in mice performing three distinct binary social discrimination
79 tasks (contexts). The same type of social stimulus served as either preferred or less-preferred stimulus in
80 all three tasks. Using this design, we could link distinct patterns of rhythmic neural activity across the
81 social brain to either stimulus identity or its valence, or to the social context. Our results reveal that the
82 pattern of coordinated oscillatory activity (coherence) in the network is strongly correlated with the social
83 context and carries information that may be used to discriminate between distinct, albeit similar, social
84 contexts. Further, we revealed that the ventral dentate gyrus (vDG), an area previously linked to
85 contextual information (Chen et al., 2020; McHugh et al., 2007), seems to play a pivotal role in
86 coordinating the coherent activity among the various regions of the social brain.

Results

Analyzing the behavior of CD1 male mice during three distinct binary social discrimination tasks

Using custom-built electrode arrays (EAr; Fig. S1A) we simultaneously acquired local field potential (LFP) signals from up to 16 brain regions at a time (cumulative count: 18 regions; Figure S1B and Table S1) during interactions of adult male mice (subjects) with various stimuli (Mohapatra et al., 2022). Specifically, we employed three distinct binary social discrimination tasks (Jabarin et al., 2021; Netser et al., 2020), namely the social preference (SP), (Fig 1A), emotional-state preference (EsP) (Fig. 1E) and sex preference (SxP) (Fig 1I) tasks (Jabarin et al., 2021). Each task comprised a five min-long baseline period involving empty chambers located at opposite corners of the arena, followed by a five min-long encounter period, when a distinct stimulus was introduced into each chamber (Netser et al., 2019). Mice performing the SP task tended to interact with social stimuli (conspecifics) for significantly more time than with objects throughout the encounter period (Fig. 1B-D). Similarly, mice performing the EsP task preferred to interact with socially isolated rather than group-housed stimuli (Fig. 1E-H), while mice performing the SxP task tended to interact more with female than with male stimuli (Fig 1I-L). Thus, in each task, the subjects discriminated between a preferred and a less-preferred stimulus. Notably, the same type of stimulus (a male group-housed mouse) that was the preferred stimulus in the SP task was the less-preferred stimulus in the other two tasks. Therefore, these set of tasks allowed us to analyze brain-wide neural activity patterns in association with either the type of stimulus (i.e., a group-housed male vs. an object/group-housed female/isolated male) or its valence (i.e., preferred vs. less-preferred), or the social context (i.e., the SP, EsP or SxP task).

We further compared multiple behavioral parameters across the various tasks. There were no significant differences between the tasks in terms of total time dedicated to stimulus investigation (Fig. 1M), the total number of transitions made by the subjects between the two stimuli (Fig. 1N) or the distance traveled by the subjects during a task (Fig. 1O). Nonetheless, the preference (reflected by the relative discrimination index, RDI) between the two stimuli was lower in the EsP task, as compared to the SP task (Fig. 1P). Overall, subject behavior was similar across the various tasks.

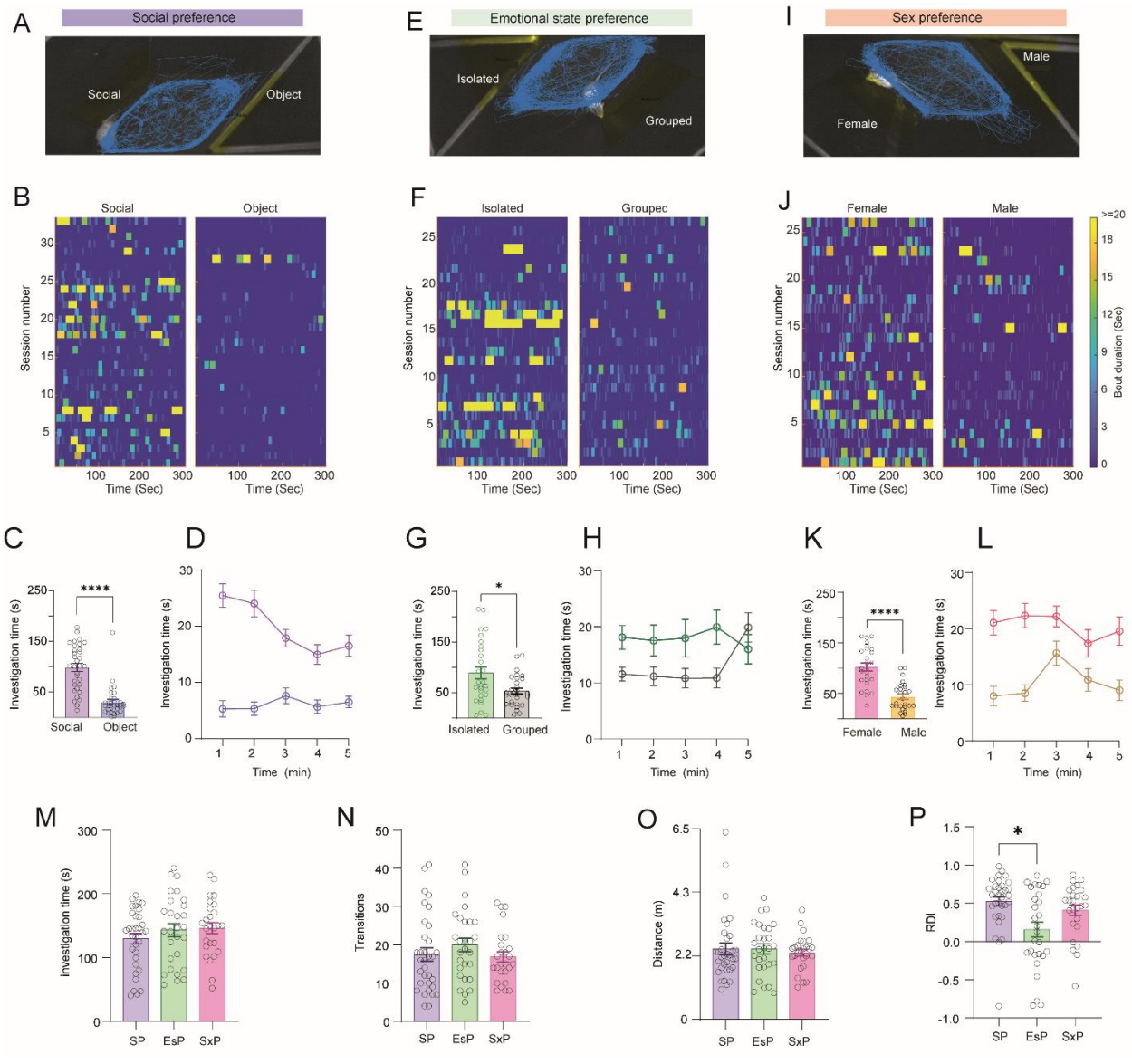

Figure 1. Similar behavior of subject mice across three binary social discrimination tasks.

A. A track of subject movements during an SP task session, super-imposed onto a picture of the arena. The two stimuli types are indicated above their chambers.

B. Heat maps of investigation bouts made by the subjects toward each of the stimuli (stimulus type is noted above) across the five min-long encounter period of the SP task, with color-coding of the investigation bout duration (see scale on the right of the panel). Each line represents a distinct session.

C. Mean (±SEM) time dedicated by a subject for investigating each stimulus during the SP task sessions shown in B. Wilcoxon matched pairs signed rank test, n = 33 sessions, W = -495, ****p<0.0001.

D. As in C, plotted vs. time using one min bins.

E-H. As in A-D, for the EsP task. Paired t-test, n = 28 sessions, t (27) =2.374, *p = 0.025.

I-L. As in A-D, for the SxP task. Paired t-test, n = 26 sessions, t (25) =5.75, ****p<0.0001.

M. Mean (±SEM) total time dedicated by a subject to investigate both stimuli during the encounter stage of a task.

N. Mean (±SEM) number of transitions between stimuli made by the subject during the encounter period of each task.

O. Mean (±SEM) distance traveled by the subjects during the encounter stage of each task.

P. Mean (±SEM) RDI for each task. Kruskal-Wallis test, n = 3 tests, 87 sessions, H = 8.509, p = 0.0142; Dunn's *post-hoc* test, *p<0.05.

Different tasks elicit different profiles of rhythmic LFP signals in multiple brain regions

The power spectral density (PSD) profiles of LFP signals recorded during the encounter period (Fig. 2A-B), differed among the various tasks performed by the same subject in a brain region-specific manner (Fig S1C). For quantitative comparison, we calculated the change in power (relative to baseline) during each task for each brain region in both the theta (ΔθP, 4-12 Hz) and gamma (ΔγP, 30-80 Hz) bands. In almost all cases, we found that the mean power of both rhythms was enhanced during the encounter period, as compared to baseline. Notably, the mean power change differed significantly among the various tasks and specific brain regions (Fig. 2C-D). The similar patterns of ΔθP and ΔγP across the various regions suggested the existence of a link between them. Accordingly, we found statistically significant correlation (Pearson's, r>0.25, p<0.05) between ΔθP and ΔγP for the SP and SxP tasks, while borderline significant correlation (r=0.45, p=0.059) was observed for the EsP task (Fig. 2E-G). Thus, when measured over the course of the entire session, both rhythms seem to be driven by the same process. When averaged across all brain regions, both ΔθP and ΔγP were highest for the SP task, compared to the other two (Fig 2H-I). Thus, despite the generally similar behavior exhibited by subjects across the tasks (Fig. 1), their system-level brain LFP signals significantly and consistently differed in power across tasks. Specifically, despite involving only one social stimulus, the SP task induced the strongest LFP rhythmicity.

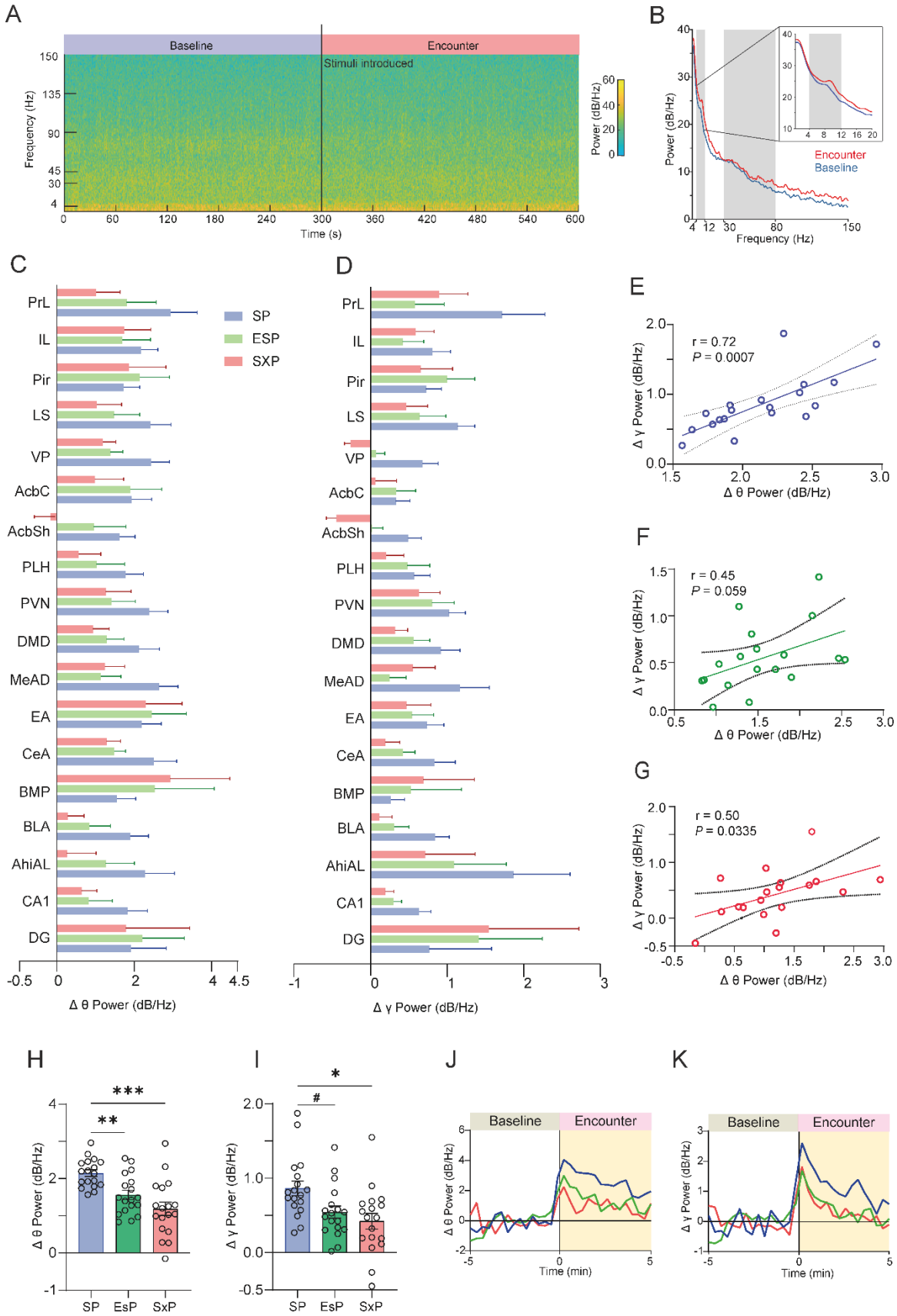
A
Baseline
Encounter
Stimuli introduced
Frequency (Hz)
Time (s)
Power (dB/Hz)
B
Power (dB/Hz)
Frequency (Hz)
Encounter
Baseline
C
D
PrL
IL
Pir
LS
VP
AcbC
AcbSh
PLH
PVN
DMD
MeAD
EA
CeA
BMP
BLA
AhiAL
CA1
DG
SP
ESP
SXP
Δ θ Power (dB/Hz)
Δ γ Power (dB/Hz)
E
r = 0.72
P = 0.0007
F
r = 0.45
P = 0.059
G
r = 0.50
P = 0.0335
H
I
J
K
SP
EsP
SxP
Baseline
Encounter
Time (min)

150

Figure 2. Brain region- and context-specific changes in the levels of theta and gamma power during a social encounter.

A. Color-coded spectrogram of LFP signals recorded in the AcbSh during the baseline (left) and encounter (right) periods of SP task. The black line at 300 s represent the time of stimuli introduction into the arena. The color-coding scale is shown on the right.

B. PSD profiles of the baseline (blue) and encounter (red) periods shown in A. The gray areas mark the theta and gamma ranges. The inset shows the theta range in higher resolution.

C. Mean (±SEM) change in theta power (ΔθP) during the encounter period, relative to the baseline period for each brain region in the three contexts (2-way ANOVA. Contexts: F (2, 659) = 3.838, p = 0.0220; Brain regions: F (17, 659) = 1.727, p = 0.0341; Interaction: F (34, 659) = 0.4548, p = 0.9970)

D. As in C, for gamma power (ΔγP; 2-way ANOVA. Contexts: F (2, 659) = 1.459, P = 0.2333; Brain regions: F (17, 659) = 2.050, P = 0.0076; Interaction: F (34, 659) = 0.5732, P = 0.9764).

E. Mean ΔγP as a function of mean ΔθP during the SP task, for each brain region. Pearson's correlation coefficient (r) and significance (p) are given.

F. As in E, for the EsP task.

G. As in E, for the SxP task.

H. Mean (±SEM) ΔθP, averaged across all brain regions, for each task. Welch's ANOVA, W (DFn, DFd) = 14.67 (2, 31.80), p <0.0001. Dunnett's T3 multiple comparisons test, SP vs. EsP, p = 0.0018; SP vs. SxP, p = 0.0002; EsP vs. SxP, P = 0.2653.

I. As in H, for ΔγP. W (DFn, DFd) = 5.134 (2, 33.65), p = 0.0113. SP vs. EsP, p = 0.0531; SP vs. SxP, p = 0.0127; EsP vs. SxP, p = 0.7467.

J. Super-imposed traces of ΔθP averaged across brain regions for the SP (blue), EsP (green) and SxP (red) tasks. Time 0 min represents the time of stimuli insertion.

K. As in J, for ΔγP.

#p= 0.053, *p<0.05, **p<0.01, ***p<0.001. See also Figs. S1, S2.

To examine the temporal dynamics of LFP rhythmicity during the various tasks, we plotted ΔθP and ΔγP as a function of time for each task and brain region. In accordance with our previous study in rats (Tendler and Wagner, 2015), we found that both ΔθP and ΔγP began to rise several seconds before stimulus introduction, peaked within 20 s from this point and gradually declined in all brain regions and tasks (Fig. S2). Thus, the dynamics of LFP rhythmicity across the session were similar among the various tasks and did not seem to reflect the behavioral dynamics (shown in Fig. 1D, H, L). We also found no significant

183 correlation (Pearson's, p>0.05) between the mean power change and speed of the subject during any task
184 for either ΔθP or ΔγP (Fig. S3A-F).
185 Overall, these results suggest that theta and gamma rhythmicity during the encounter period are driven
186 by an internal brain state of arousal that shows similar temporal dynamics across tasks, independent of
187 the behavioral dynamics.
188
189 ***LFP power changes during stimulus investigation are differentially modulated across brain regions and***
190 ***tasks***
191 Despite the uniform dynamics of LFP rhythmicity in the social brain during the encounter period, it may
192 be differentially modulated during specific behavioral events, such as stimulus investigation. We thus
193 examined the possibility that during investigation bouts, ΔθP and ΔγP (henceforth termed $^{\Delta}$θP and $^{\Delta}$γP)
194 differ between the various stimuli and tasks. As exemplified by signals recorded from the amygdalo-
195 hippocampal area (AhiAl) shown in Fig. 3A-F, a Z-score analysis revealed elevation in theta power during
196 investigation bouts towards social but not the object stimuli in the SP task, during investigation of both
197 stimulus types in the EsP task and during investigation of female but not male stimuli in the SxP task. Very
198 similar results were obtained for gamma power (Fig. S4A-F). This analysis thus suggests a bias towards
199 specific stimuli in a task-specific manner. Interestingly, even though the same type of stimulus (a group-
200 housed male) was used in all tasks, this stimulus elicited a clear elevation in LFP rhythmicity only during
201 the SP and EsP tasks but not during the SxP task. These results suggest that at least for the AhiAl, the
202 change in LFP rhythmicity was not dictated by either the stimulus type nor by its valence.
203 To explore the bias in LFP rhythmicity in each task, we calculated the difference in $^{\Delta}$θP and $^{\Delta}$γP between
204 the two stimuli separately for each brain region. Since a possible bias of LFP rhythmicity in a given brain
205 region may be associated with a behavioral bias towards a specific stimulus, we examined the correlation
206 between the two variables. To this end, we correlated the $^{\Delta}$θP bias (preferred – less-preferred) to the RDI
207 values of each task. We found a negative correlation in a specific set of brain regions (i.e, extended (EA)
208 and medial (MeAD) amygdala, lateral septum (LS), paraventricular hypothalamic nucleus (PVN),
209 infralimbic (IL) and prelimbic (PrL) prefrontal cortex) only for the SP task. In contrast, a positive correlation
210 was found in a distinct set of brain regions (nucleus accumbens shell (AcbSh), AhiAl, ventral pallidum (VP)
211 and dorsomedial hypothalamic nucleus (DMD)) during the EsP and SxP tasks. Specifically, the VP exhibited
212 a very strong and highly significant linear correlation with RDI values during both the EsP and SxP tasks
213 (Fig 3G). These results suggest a link between stimulus-specific bias in $^{\Delta}$θP and behavioral preference in a
214 task-specific manner.

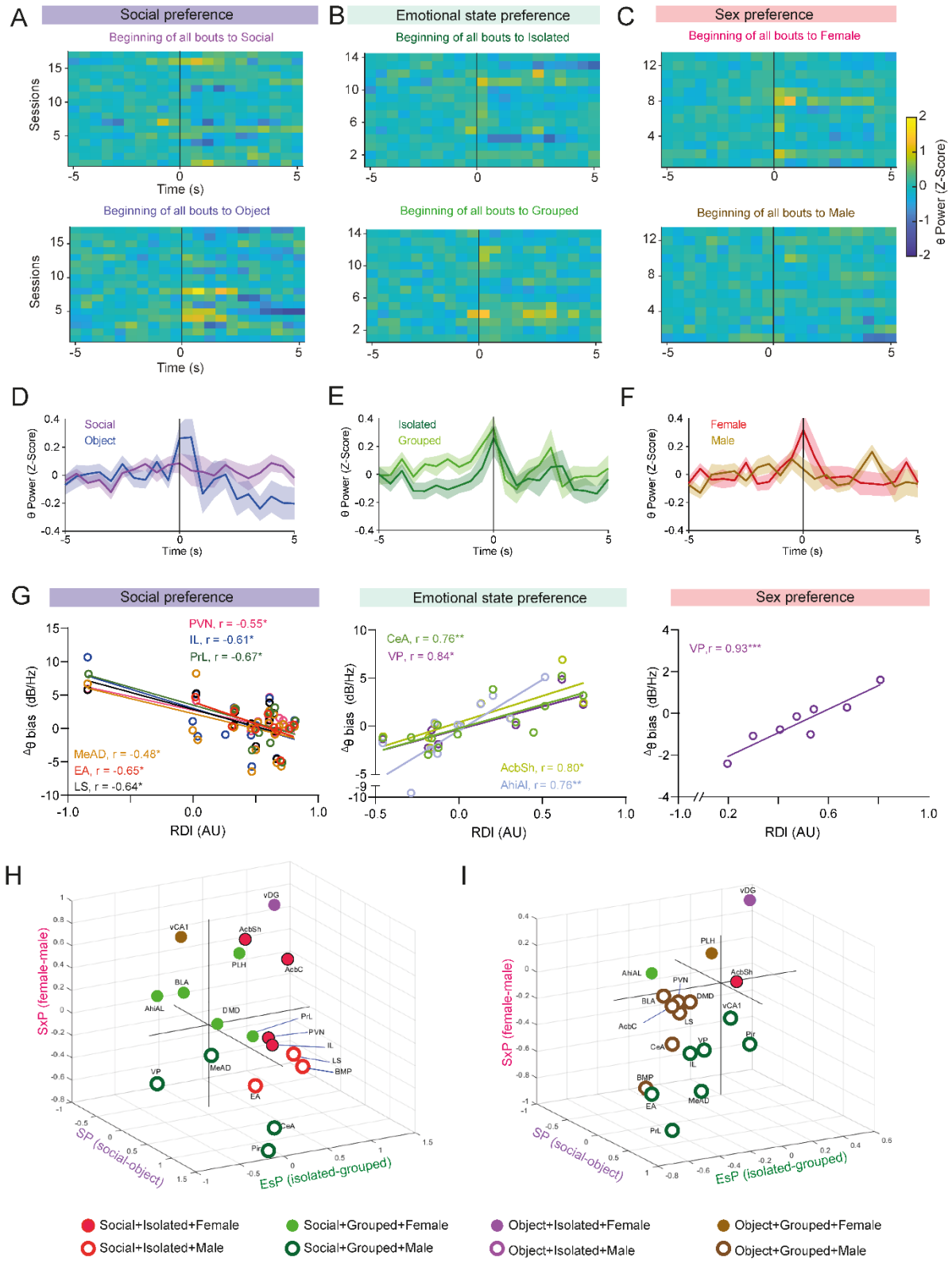

Figure 3. Stimulus- and task-specific LFP power changes during investigation bouts.

A. Heat maps of average theta power in AhiAl, before and during social investigation bouts of subjects with social (above) and object (below) stimuli. Each row represents the mean Z-score of all bouts in a single session (using 0.5 s bins). Time '0' represents the beginning of the bout. The color code scale is on the right.
B. As in A, for investigation bouts of isolated (above) and grouped (below) social stimuli during EsP tasks.
C. As in A, for investigation bouts of female (above) and male (below) social stimuli during SxP tasks.
D. Mean (±SEM) Z-score trace of the data shown in A for both stimuli.
E. As in D. for the data shown in B.
F. As in D, for the data shown in C.
G. Correlation between mean change in theta power during investigation bouts ($^{\Delta}\theta P$) in specific brain regions and RDI values during the various tasks. Only statistically significant linear correlations are shown.
H. A 3D plot of the mean difference between preferred and less-preferred stimuli in $^{\Delta}\theta P$. Each dot represents a given brain region, color- and shape-coded according to the combined bias across all tasks.
I. As in B, for $^{\Delta}\gamma P$.

See also Fig. S4.

To further explore this link, we plotted $^{\Delta}\theta P$ bias across all tasks on a 3D plot, separately for each brain region. We found that almost no region showed bias towards the object stimulus in the SP task, with the various regions being equally distributed between the two stimuli in the EsP and SxP tasks (Fig. 4B). In contrast, when $^{\Delta}\gamma P$ was analyzed (Fig. 4C), we observed an opposite picture. Here, almost all brain regions exhibited stronger responses to the grouped and male stimuli in the EsP and SxP tasks, yet were rather equally distributed between the two stimuli in the SP task. Thus, for $^{\Delta}\gamma P$, most brain regions (14/18) were equally divided between those biased towards less-preferred stimuli (i.e., object+grouped+male) and those biased towards the type of stimulus used in all three tasks (i.e, social+grouped+male). The probability of such an arrangement to occur by chance is smaller than 0.001 (1-binomial test) for each of these two groups. The results thus suggest that a bias in gamma power is mostly associated with the characteristics (i.e, valence or type) of the stimulus. They also generally demonstrate opposite stimulus-dependent bias patterns between the theta and gamma rhythms during stimulus investigation, in contrast to their significant correlation when measured during the entire encounter period (Fig. 2E-G). This implies the existence of an independent active state in the social brain during stimulus investigation. Notably, of

249 all brain regions considered, the vDG stood out as the only region biased to the combination of
250 object/isolated/female stimuli. Moreover, this region showed an extreme bias for all these stimuli in both
251 $^{\Delta}\theta P$ and $^{\Delta}\gamma P$. These results point to a unique position for the vDG in the social brain, as also supported by
252 results presented below.

253 ***Social encounters modulate coherence between brain regions in a social context-dependent manner***

254 Synchronous activity (coherence) enhances effective communication between neuronal groups in
255 different brain regions and dynamically binds them into functional networks (Fries, 2015). We, therefore,
256 examined coherence in LFP signals between each pair of brain regions recorded by us, in both the theta
257 and gamma bands. During the baseline period, the mean theta coherence between all pairs of brain
258 regions (99 pairs) was similar across all tasks (Fig. 4A). Thus, the subjects displayed similar global brain
259 synchronization while exploring the arena without stimuli, in all tasks. However, the change in theta
260 coherence (ΔθCo) measured during the encounter period differed significantly between tasks. While
261 almost all pairs of brain regions exhibited increased theta coherence during the SP task, we observed
262 significantly milder increases during EsP and SxP tasks, with many paired regions showing reduced
263 coherence (Fig. 4B, E-G). Similar relationships among tasks were observed for changes in gamma
264 coherence (ΔγCo), although here the general tendency was one of decreased coherence during the
265 encounter period (Fig. 4C-G). Notably, there was almost no correlation between the baseline period
266 coherence and the change in coherence during the encounter period for any task (apart a weak correlation
267 for SP gamma coherence; $r=-0.21$, $p=0.0111$; not shown). This suggests that the encounter-induced
268 coherence change represents an internal state, independent of the resting state. Finally, when calculating
269 the correlations across all paired regions in ΔθCo between the various tasks, we found a statistically
270 significant high correlation between SxP and EsP, while no correlation was found between SP and SxP. A
271 milder but significant correlation was found between SP and ESP (Fig. 5H). In contrast, all correlations
272 were found significant for ΔγCo. These results suggest a gradual shift from SP to ESP and to SxP when in
273 ΔθCo brain pattern is measured across the whole encounter.

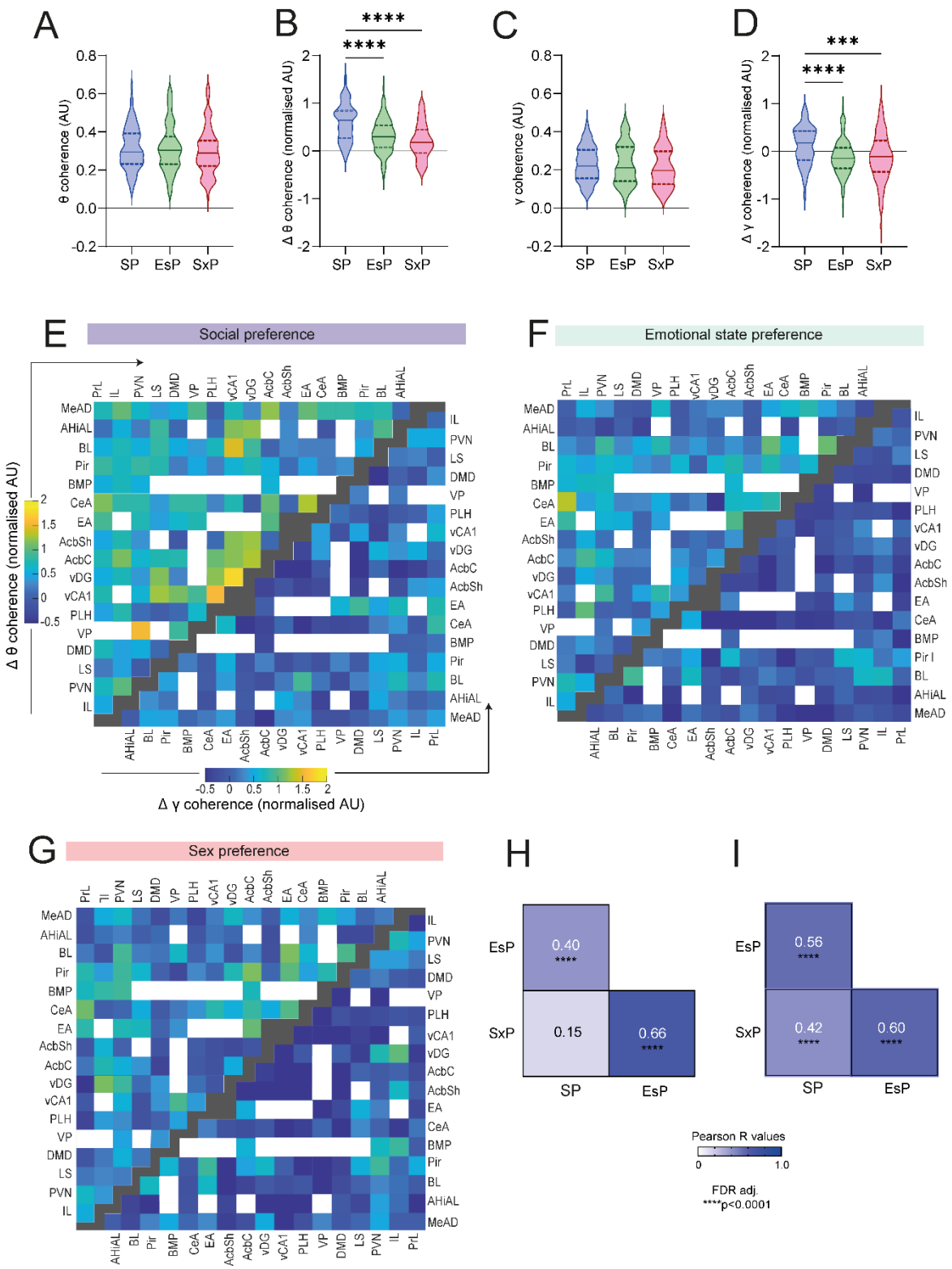
A
θ coherence (AU)
SP
EsP
SxP
B
****
****
Δ θ coherence (normalised AU)
C
γ coherence (AU)
D
***
****
Δ γ coherence (normalised AU)
E
Social preference
Δ θ coherence (normalised AU)
Δ γ coherence (normalised AU)
F
Emotional state preference
G
Sex preference
H
EsP
SxP
0.40
****
0.15
0.66
****
I
0.56
****
0.42
****
0.60
****
Pearson R values
0
1.0
FDR adj.
****p<0.0001

274

Figure 4. Social encounters modulate the coherence between brain regions in a social context-dependent manner.

A. Mean theta coherence during the five min-long baseline period before the encounter period for each task, across all (n=99) pairs of brain regions recorded during all tasks (Kruskal-Wallis test, H = 0.75, *P* = 0.687).

B. As in A, for mean normalized change in theta coherence (ΔθCo) during the encounter period. Note the significant difference between the SP and other tasks (****p<0.0001, Dunn's *post-hoc* test following the main effect in a Kruskal-Wallis test).

C-D. As in A and B, for gamma coherence (***p<0.001, ****p<0.0001).

E. Color-coded matrix of the mean normalized ΔθCo (upper left) and ΔγCo (lower right) values for all pairs of brain regions in the SP task. Empty spots represent brain region pairs with fewer than five recorded sessions. Black spots separate between the ΔθCo and ΔγCo matrices.

F. As in E, for EsP.

G. As in E, for SxP.

H. Coefficients and significance of Pearson's correlations of ΔθCo across all coupled brain regions for each pair of tasks (****p<0.0001).

I. As in H, for ΔγCo.

See also Fig. S5.

We, therefore, examined the encounter-induced coherence changes for each brain region separately, by comparing the change in coherence between a given region and all other regions across tasks in the theta (Fig. S5A) and gamma (Fig. S5B) bands. We found that differences between tasks were brain-region specific, with most (13/18) regions showing significant differences between at least two tasks in ΔθCo and almost half (8/18) showing differences in ΔγCo. Notably, in all cases, we found significantly higher coherence changes during the SP task, as compared to at least one task, and in many cases, to both other tasks. Thus, a subset of the recorded brain regions displayed differential changes in theta or gamma coherence among the social contexts, with this change being majorly increased in the SP task, as compared to the other two tasks.

Brain-wide coherence changes during investigation bouts reflect the social context

To explore possible modulation of coherence during investigation bouts, we calculated the mean $^{\Delta}\theta$Co between each pair of brain regions during all investigation bouts towards a given stimulus, similarly to

how we analyzed power changes (Fig. 3). Since data had been collected for a large number of brain-region pairs (overall, 99 pairs recorded across all tasks for at least 5 sessions per task), we focused on pairs with a mean that crossed a cutoff value ± 1.5*standard deviation (SD) for each stimulus (about 20% of the pairs). When plotting differences in $^{\Delta}\theta Co$ between the two stimuli in each task on a 3D plot (Fig. S6A-B), we observed a much wider distribution than was found for power (Fig. 3H-I), suggesting distinct principles of distribution. To further explore this possibility, we examined all pairs of brain region that passed the aforementioned threshold, separately for each stimulus (Fig. 5A). Surprisingly, the three stimuli of the same type (i.e, social, grouped, male) did not share even a single pair of brain regions that passed the $^{\Delta}\theta Co$ cutoff value. Similarly, the preferred stimuli (i.e, social, isolated, female) also did not share even a single pair among them. In contrast, multiple pairs of brain regions shared similar changes in theta coherence between both stimuli used in each task (Fig. 5A). For example, CeA-PrL and MeAD-VP showed increased coherence for both social and object stimuli, BLA-LS and EA-Acbc showed increased coherence for both isolated and grouped stimuli and Pir-AcbC and EA-AcbC exhibited the strongest increase in theta coherence for both male and female stimuli. Similar results were observed for gamma coherence (Fig. S6C). Thus, changes in coherence seem to be dictated by the social context rather than by stimulus characteristics, such as its type or valence.

For quantitative examination of this possibility, we calculated the correlation across all brain regions for either $^{\Delta}\theta Co$ (Fig. 5B) and $^{\Delta}\gamma Co$ (Fig. 5C), between pairs of stimuli which share common context, type or valence. We found strong and highly significant correlations between all pairs of stimuli used in the same task (sharing context). In contrast, among the three stimuli of the same type, only grouped (ESP) and male (SxP) showed significant correlation. Similarly, among preferred stimuli, only isolated (EsP) and female (SxP) showed significant correlations. Notably, in both of these cases the correlation was weaker than the correlation between any pair of stimuli sharing the same context (Fig. 5B). Similar results were found for $^{\Delta}\gamma Co$ (Fig. 5C). Thus, we conclude that the coherence changes in both theta and gamma rhythms during stimulus investigation had the strongest association with the context of the social interaction, relative to any characteristic of the stimulus.

Finally, we employed a Decision trees (multi-class Random forest) classifier to examine if $^{\Delta}\theta Co$ and $^{\Delta}\gamma Co$ contain information which may be used to discriminate between the various contexts or stimuli. First, we validated that the model achieved good (~60%) and significant accuracy in predicating the social stimulus vs. object in the SP task using either $^{\Delta}\theta Co$ or $^{\Delta}\gamma Co$. Notably, the classification of the object vs. social was not accurate, suggesting that the presence of the social stimulus (social context) mask the object classification (Fig. S7A-B). Then, we used the same model for predicting the social context and found that

339 using $^{\Delta}\theta$Co (Fig. 5D), but not $^{\Delta}\gamma$Co (Fig. 5E), allowed the model to predict the right context better than any
340 other context, and that this prediction was the only one achieving more than a chance level (33.3%)
341 accuracy (although only SxP classification got statistical significance). In contrast, the same model worked
342 poorly for predicting stimulus identity among all six stimuli (Fig. S7C-D). Using the LFP theta power ($^{\Delta}\theta$P)
343 for predicting the social context by the same model achieved good and significant classification only for
344 the SP (Fig. S7E), while using both theta power and coherence allowed accurate prediction of both SP and
345 SxP contexts (Fig. S7F). These results suggest that LFP rhythmicity in the theta range, especially the
346 coherence of between the various brain regions, is informative regarding the social context of the animal
347 more than regarding the identity or valence of the social stimuli.

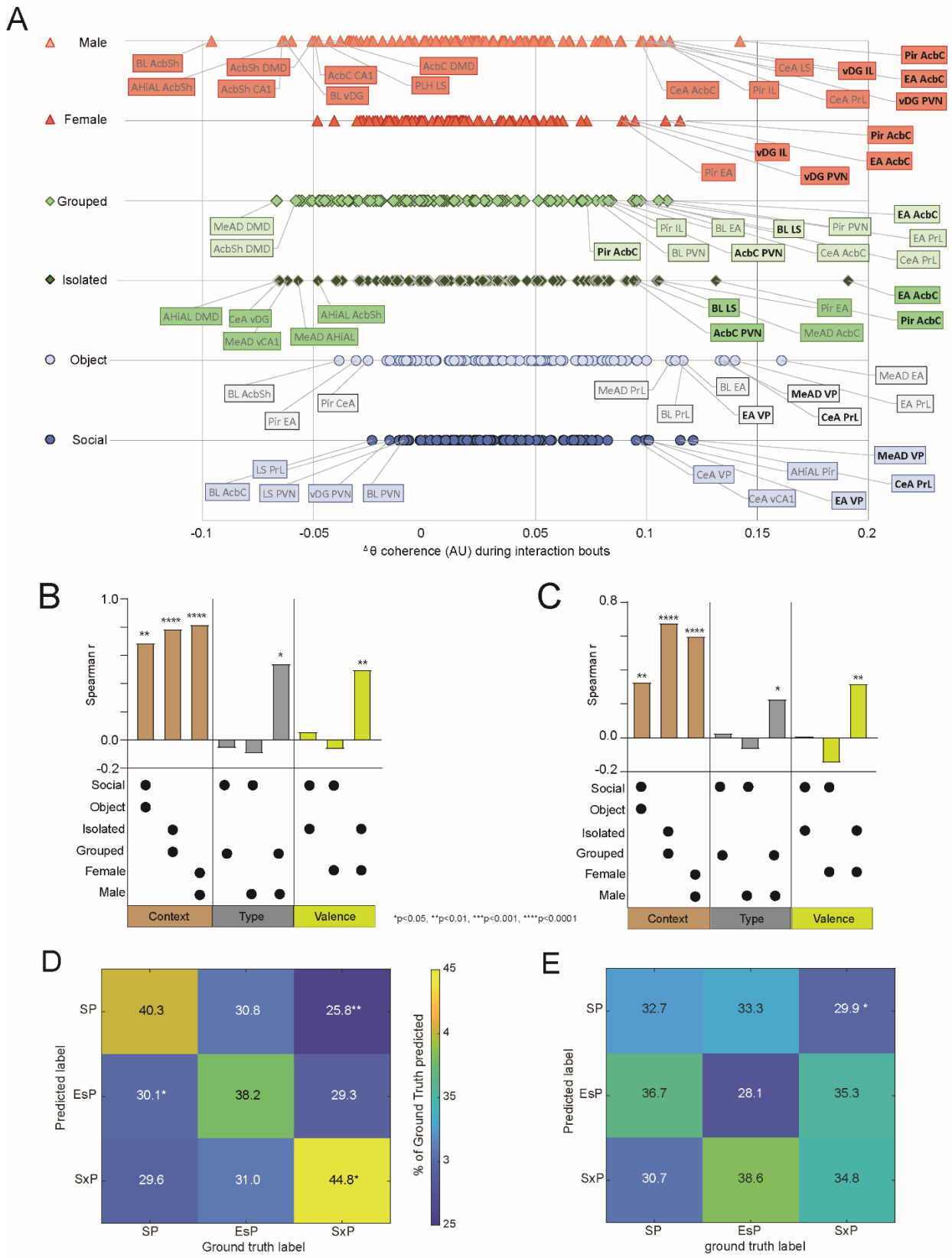

Figure 5. Coherence changes during social investigation are informative regarding the social context

350 A. Distribution of changes in theta coherence during investigation bouts ($^{\Delta}\theta Co$) between each pair of
351 brain regions, plotted separately for each stimulus used in the SP (blue), EsP (green) and SxP (red)
352 tasks. The names of brain region pairs which passed the mean cutoff value ±1.5*SD are labeled, with
353 those showing similar $^{\Delta}\theta Co$ for both stimuli in the same task in bold.
354 B. Spearman's correlation coefficients of mean $^{\Delta}\theta Co$ across all paired brain regions, for couples of stimuli
355 which were either used in the same task (left, brown bars), of the same type (middle, gray) or having
356 the same valence (right, yellow). The correlated two stimuli are denoted by asterisk below each bar,
357 while the statistical significance of the correlation is marked above the bars.
358 C. As in B, for $^{\Delta}\gamma Co$.
359 D. A color-coded confusion matrix for a multi-class Random forest classifier employed for predicting the
360 social context from $^{\Delta}\theta Co$ values across all brain regions and stimuli. The scale of the accuracy's color
361 code is shown to the right. The percentage of cases a label was predicted for each ground truth are
362 marked in the middle of each spot. *p<0.05, **<0.01, Mann-Whitney test.
363 E. As in D, for $^{\Delta}\gamma Co$.
364 See also Figs. S5, S6.
365
366 ***Analysis of Granger causality suggests that specific brain regions serve as hubs***
367 The coherent LFP rhythmicity in the social brain can be dominated by specific regions serving as hubs,
368 thereby preceding other regions in terms of rhythmic neural activity. To identify hub candidate regions,
369 we first selected brain regions which are statistically over-represented (see Methods) among pairs of
370 regions exhibiting strong (mean ± 1.5*SD) bias in any task, separately for $^{\Delta}\theta Co$ (Fig. 6A) and $^{\Delta}\gamma Co$ (Fig. 6B).
371 We then examined the dependence of LFP rhythmicity of each of these regions in terms of preceding
372 rhythmicity of other regions by calculating the change in Granger causality (GC) (Barnett and Seth, 2014)
373 during the encounter period (Fig. 6C-E). We found distinct patterns of statistically significant changes in
374 GC (in the encounter vs. baseline periods) between the various tasks (Fig.6-H). Some regions, however,
375 presented significant GC changes in all tasks, suggesting that they might function as hubs. For example,
376 vDG and AcbC participated in significant GC changes in both theta and gamma rhythms in all tasks. At the
377 same time, PrL and AhiAl were explicitly involved in theta GC changes in all tasks. Interestingly, theta GC
378 changes from vDG to AhiAl increased during a SP task but decreased during a EsP task, while theta GC
379 changes from PrL to vDG decreased during both EsP and SxP tasks. These results suggest that these brain
380 regions dictate LFP rhythmicity in the social brain during social investigation.

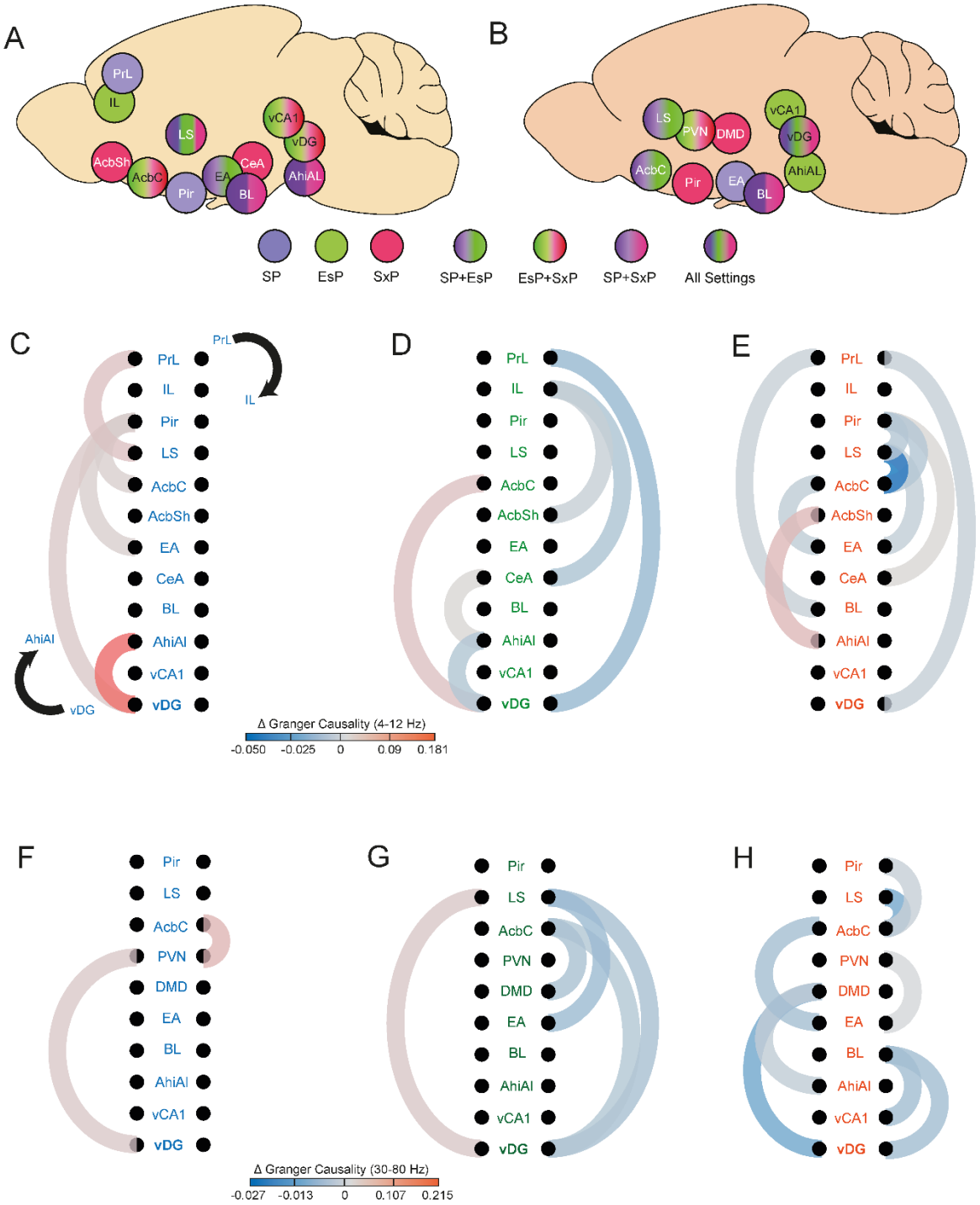

Figure 6. Distinct patterns of changes in Granger causality during the encounter period among tasks.

A. Schematic representation of the brain regions over-represented among the brain region pairs that exhibited strong (mean ± 1.5*SD) theta coherence bias towards one of the stimuli in any task. The regions are color-coded according to the task in which they were over-represented.

B. As in A, for gamma coherence.

C. Schematic representation of significant changes (in encounter vs. baseline periods) in theta band GC during a SP task, among the regions listed in A. The direction of the GC changes in shown by a black arrow (top to bottom on the right and bottom to top on the left).

D. As in C, for EsP.

E. AS in C, for SxP.

F-H. As in C-E, for gamma band

Context-specific synchronization of LFP rhythmicity in the ventral dentate gyrus with precise behavioral events

To further examine the candidate hub regions, we exploited our ability to determine the exact timing of each investigation bout to quantify the synchronized modulation of LFP rhythmicity, relative to these events. Thus, we compared the modulation of theta and gamma power in all regions associated with significant GC changes (Fig. 6) relative to a defined battery of specific behavioral events (Fig. 7A). These events included the beginning and end of short (<2 s) and long (>2 s) investigation bouts towards specific stimuli, as well as transitions between stimuli. We found a main effect in ANOVA for multiple events, although in most cases, none of the regions showed significance *in post-hoc* analysis (see Table S2). One region, the vDG, did, however, exhibit significant differences between events. The vDG displayed significantly higher theta and gamma powers at the end of long investigation bouts of social stimuli, as compared to object stimuli, specifically in the SP task (Fig. 7B-G and S7A-B). The same region also exhibited decreased theta and gamma powers at the beginning of transitions from isolated to grouped stimuli, as compared to non-transitional bouts, specifically in the EsP task (Fig. 7H-M and S7C-D).

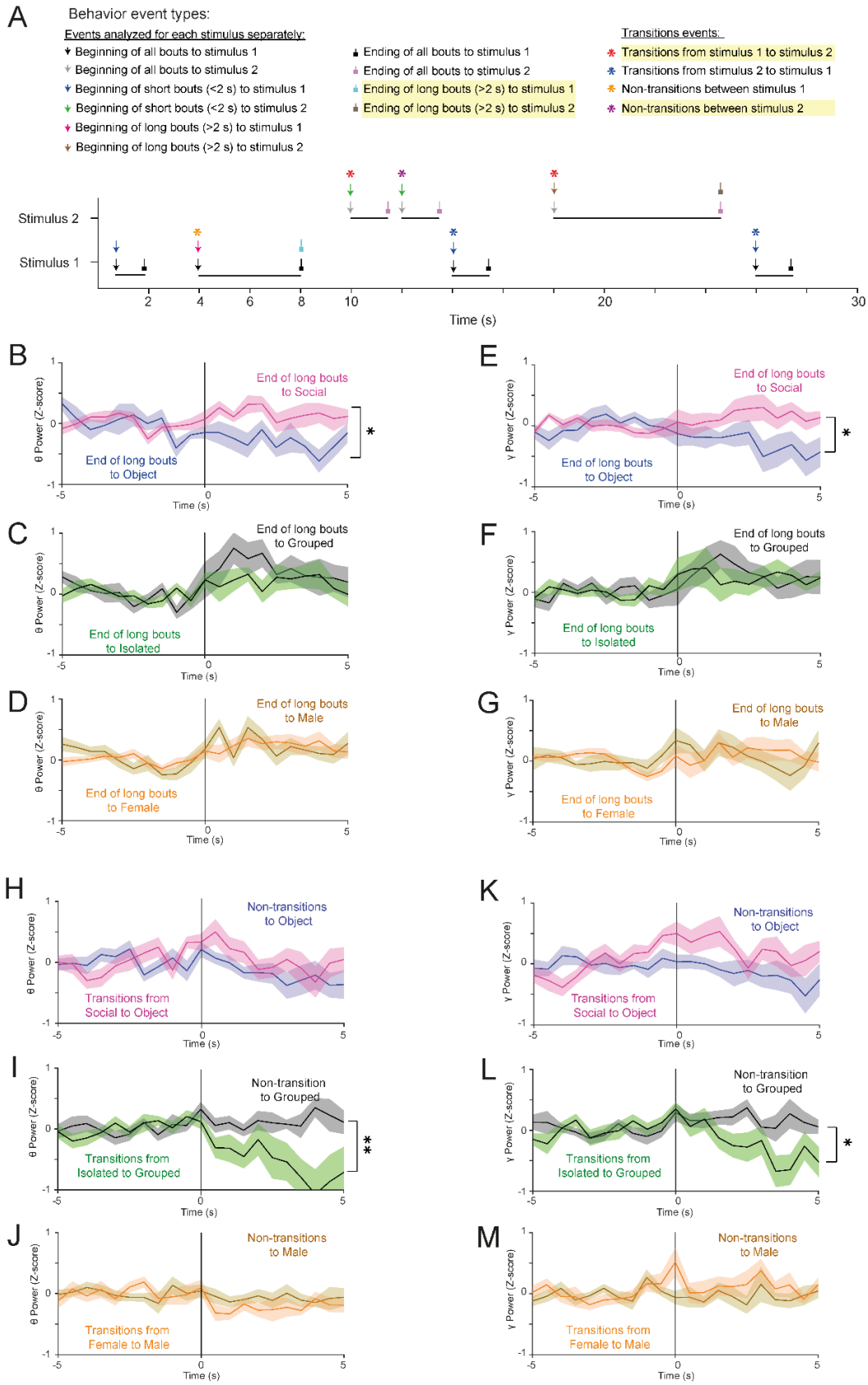
A
Behavior event types:
Events analyzed for each stimulus separately:
Beginning of all bouts to stimulus 1
Beginning of all bouts to stimulus 2
Beginning of short bouts (<2 s) to stimulus 1
Beginning of short bouts (<2 s) to stimulus 2
Beginning of long bouts (>2 s) to stimulus 1
Beginning of long bouts (>2 s) to stimulus 2
Ending of all bouts to stimulus 1
Ending of all bouts to stimulus 2
Ending of long bouts (>2 s) to stimulus 1
Ending of long bouts (>2 s) to stimulus 2
Transitions events:
Transitions from stimulus 1 to stimulus 2
Transitions from stimulus 2 to stimulus 1
Non-transitions between stimulus 1
Non-transitions between stimulus 2
Stimulus 2
Stimulus 1
Time (s)
B
θ Power (Z-score)
End of long bouts to Social
End of long bouts to Object
Time (s)
E
γ Power (Z-score)
End of long bouts to Social
End of long bouts to Object
C
End of long bouts to Grouped
End of long bouts to Isolated
F
End of long bouts to Grouped
End of long bouts to Isolated
D
End of long bouts to Male
End of long bouts to Female
G
End of long bouts to Male
End of long bouts to Female
H
Non-transitions to Object
Transitions from Social to Object
K
Non-transitions to Object
Transitions from Social to Object
I
Non-transition to Grouped
Transitions from Isolated to Grouped
L
Non-transition to Grouped
Transitions from Isolated to Grouped
J
Non-transitions to Male
Transitions from Female to Male
M
Non-transitions to Male
Transitions from Female to Male

408

409 **Figure 7. Context-specific differences in vDG LFP rhythmicity in specific behavioral events**

410 A. Color-coded scheme of specific behavior event types, with ↓ indicating the beginning of an event, ⊥
411 indicating the end of the event and * indicating the beginning of event after transition. Events showing
412 significant differences in vDG LFP power are highlighted in yellow.

413 B. Super-imposed traces of the mean (±SEM) Z-score of changes in vDG theta power at the end of long
414 bouts towards either a social stimulus (pink) or an object stimulus (purple) in the SP task. Time 0
415 represents the end of the bout, while the 5 s period before time 0 was considered as baseline. *p<0.05,
416 according to Student's t-test between the mean Z-score values averaged over the last 2 s of the traces.

417 C. As in B, for gamma power in the vDG during SP tasks.

418 D-E. As in B-C, for the EsP task.

419 F-G. as in B-C, for the SxP task.

420 H-I. As in B-C, for changes in LFP power at the beginning of transitional vs. non-transitional investigation
421 bouts of social and object stimuli across SP task sessions.

422 J-K. As in H-I, for the EsP task. **p<0.01 by a Mann-Whitney test following the main effect in ANOVA.

423 L-M. As in H-I, for the SxP task.

424 See also Fig. S8.

425

426 These results, together with those shown in Fig. 3B-C and Fig. 6, suggest that the vDG functions as a hub
427 in the social brain network by dictating the rhythmic neural activity of the network in a social context-
428 dependent manner. In accordance with this idea, a descriptive plot of the change in theta and gamma
429 coherence during investigation bouts between the vDG and all other regions reveals a pattern which is
430 highly stimulus- and social context-dependent (Fig. 8).

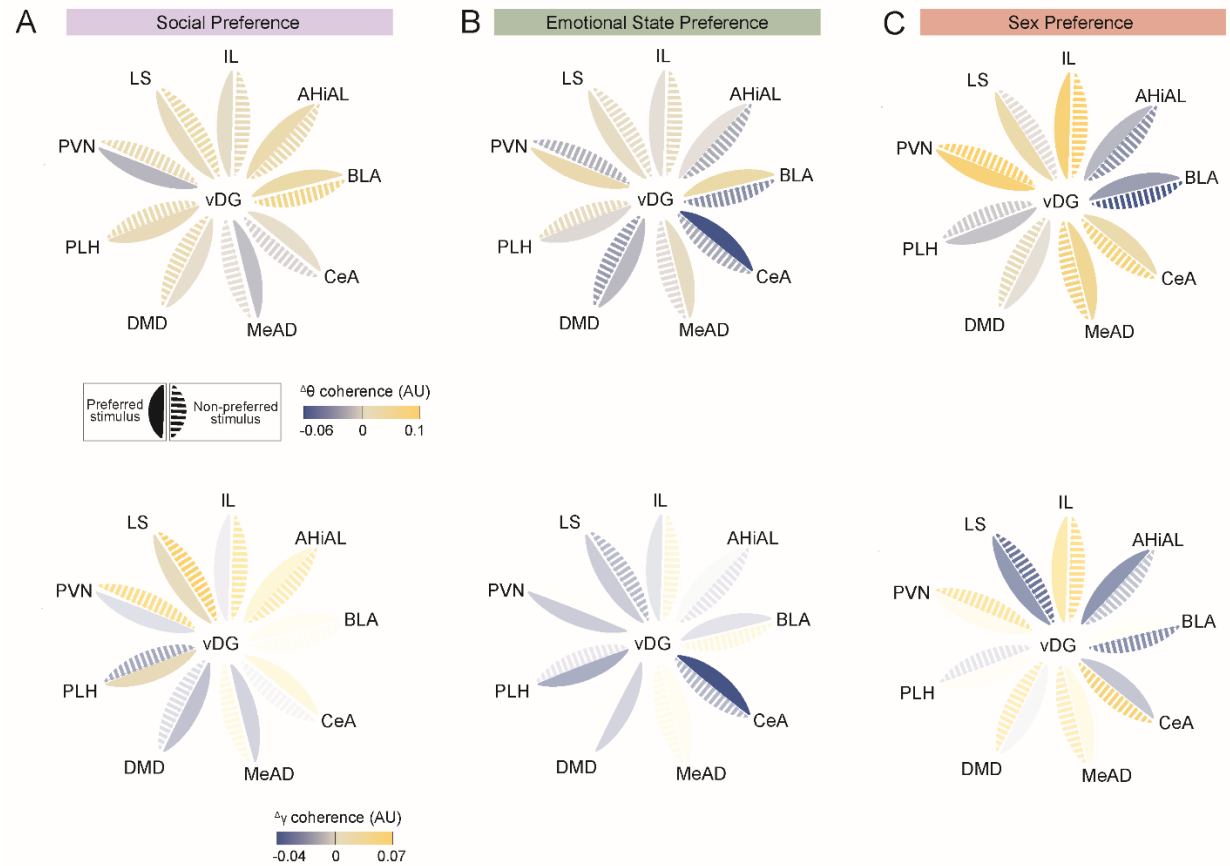

Figure 8. Stimulus- and social context-dependent patterns of coherence changes between the vDG and other brain regions

A. Color-coded flower plots of the change in theta ($^{\Delta}\theta$Co, upper plot) and gamma ($^{\Delta}\gamma$Co, lower plot) coherence during investigation bouts made in the course of SP sessions towards the preferred (blank leaves) and less-preferred (dashed leaves), between the vDG and all other regions simultaneously recorded with it during at least five sessions across all tasks.

B. As in A, for EsP sessions.

C. As in A, for SxP sessions.

Discussion

In this study, we used multi-site electrophysiological recordings from the murine social brain to seek system-level neural correlates of three distinct aspects of social interaction, namely, the identity of the social stimulus, its relative valence (preference) and the social context. To distinguish between these three aspects, we relied on three social discrimination tasks (i.e., SP, EsP, and SxP) in which male mice clearly prefer one of two distinct stimuli. This design enabled us to employ the same type of social stimulus, a novel group-housed male mouse, in all three tasks, with this stimulus being the preferred stimulus in the SP task and the less-preferred stimulus in the other two tasks. Importantly, all three tasks took place in the same experimental arena, which enables uniform interactions between the subject and the stimuli, i.e., stimulus investigation by the subject (Netser et al., 2019). Consequently, as much as we could measure, subject behavior was almost identical in all three tasks. Therefore, behavioral differences cannot explain the significant differences in the patterns of rhythmic LFP signals observed among the different tasks.

We analyzed LFP signals at three different time resolutions, specifically, across the session, during investigation bouts, and during specific behavioral events, such as at the beginning and end of long or short investigation bouts. When analyzing the power of both theta and gamma rhythms over an entire session, some aspects seemed to be dictated by a general state of arousal. In accordance with previous studies by us and others (Kuga et al., 2022; Tendler and Wagner, 2015), virtually all brain regions exhibited higher level of theta and gamma power during the encounter period, as compared to the baseline period. Our observation that the level of enhanced power was both brain region- and task-specific strongly suggests that this was not caused by enhanced electrical noise or any other artifact but rather by a genuine internal state of the animal. The uniform dynamics of both theta and gamma power changes across all brain regions and tasks during the encounter period further supports the existence of an internal arousal changes which are independent of behavioral dynamics or context. Notably, we observed significant correlations across brain regions between theta and gamma power changes in all tasks, suggesting that both rhythms are similarly influenced by the internal state. In agreement with our previous studies in both rats and mice (John et al., 2022; Tendler and Wagner, 2015), theta and gamma power maintained their high levels for a time, even after removal of the stimuli from the arena (not shown), further supporting the presence of an internal state of arousal, which slowly fades away. This state did not seem to be induced by subject movement, as we found no correlation between subject speed and changes in theta or gamma power for any brain region.

While the dynamics of the internal arousal state seemed to be similar across the distinct contexts, other aspects of the general (session-wise) changes in theta and gamma power exhibited context-specific characteristics. For example, the general changes in both power and coherence were highest in the SP task, suggesting a higher level of arousal. These results are somewhat surprising, given how the SP task involved only one social stimulus and assuming that among the various stimuli tested, the female would be the most attractive to the male subjects. Our interpretation is that the SP task is simpler in terms of conflicting tendencies, as it requires the animal to choose between an inanimate object and a conspecific, while the other two tasks involve two conspecifics, thereby presenting the subject with a more challenging dilemma. The higher confidence of the subject during the SP task is in accord with the simpler pattern of theta coherence changes observed during this task (seen as a general increase across almost all brain region pairs). Overall, these suggests that the arousal level may distinguish between some contexts, which is in accordance with the ability of the Random Forest model to predict only the SP context based on the arousal-induced LFP power. Nevertheless, the changes in theta and gamma power across the encounter period did not differ between the EsP and SxP tasks, and thus cannot be the sole basis for the context-specific responses to social cues.

Notably, a recent paper (Mague et al., 2022) that employed similar recordings during the SP test, used the power, coherence and GC data (termed *Electome network*) from various regions of the social brain in a machine-learning model to discriminate between social and object investigation. In accordance with our results, this study reported that the model's precision was higher for the social than for the object, thus suggesting that the social stimulus masks the object, which may be attributed to the social context.

Analysis of the power change, specifically during stimulus investigation bouts, yielded a different picture than did session-wide analysis. First, we found no correlation between theta and gamma power changes during these periods, suggesting a distinct state of active sensing which characterizes stimulus investigation. Moreover, although both theta and gamma power changes across brain regions showed bias to specific combinations of stimuli, they did so in distinct manners. While theta power was biased towards the preferred stimulus in the SP task, with almost no region (other than hippocampal areas) showing a preference for object stimuli, the gamma power was clearly biased towards the less-preferred stimuli in the ESP and SxP tasks (grouped and male stimuli), while showing a mixed preference between stimuli in the SP task. Thus, as related to gamma power, the social brain seems to be divided between regions associated with the valence of stimulus (biased towards less-preferred stimuli) and brain regions associated with the type of stimulus. It should be noted that theta rhythmicity is thought to reflect top-down processes, such as arousal and attention (Colgin, 2011; Gordon, 2011; Harris and Gordon, 2015b),

505 which are regulated by brain wide-active neuromodulators and recruit distributed brain networks
506 (Clayton et al., 2015; Fiebelkorn and Kastner, 2019; Helfrich et al., 2019; Karakas, 2020; Knyazev, 2007).
507 In contrast, gamma rhythmicity is considered a bottom-up process (Buzsaki and Wang, 2012; Headley and
508 Pare, 2013), associated with the synchrony of local inhibitory networks (Benchenane et al., 2011; Buzsaki
509 and Wang, 2012; Headley and Pare, 2013; Palva and Palva, 2018). This distinction may explain why theta
510 and gamma rhythms reflect stimulus characteristics in an opposing manner.
511 In accordance with our hypothesis, that coherent theta and gamma rhythms couple various regions of the
512 social brain in a social context-dependent manner, we found that the correlation in the coherence change
513 during stimulus investigation was strongest between the two stimuli in each task, even the EsP and SxP
514 tasks. In contrast, there were weaker correlations, if any, among the three stimuli of the same type (social,
515 grouped, male) or the preferred stimuli (social, isolated, female). The fact that the same correlation
516 pattern was observed for both theta and gamma coherence supports the validity and significance of the
517 observation. Moreover, using a Decision Tree classifier, we demonstrated that the theta coherence
518 between the recorded areas could generate predictions regarding the social context, but not the specific
519 stimulus, which are accurate above the chance level. The limited accuracy of the model may be attributed
520 to the restricted number of recorded regions. Thus, we expect that a more comprehensive analysis of the
521 coherence within the social brain will be able to generate highly accurate prediction of the social context.
522 Moreover, GC analysis, representing causal time relationships between various brain regions, also
523 suggests distinct patterns of changes across the various contexts. Altogether, these results support the
524 idea that the social brain processes information during stimulus investigation in a context-dependent
525 manner dictated by the context-dependent pattern of coherence within the network. Such a mechanism
526 may explain how the same stimulus induces distinct patterns of brain activity in different social contexts,
527 which then elicits distinct behavioral responses to a stimulus.
528 Finally, the coherence change and GC analyses led us to identify a small subset of brain regions that seem
529 to highly influence the network during the various tasks. Of these, the vDG and AcbC were involved in
530 significant GC changes during all tasks in both the theta and gamma bands, and thus may serve as hubs
531 that dictate the activities of other regions. Analysis of LFP power in relation to a battery of specific
532 behavioral events demonstrated that while the small group of brain regions considered showed
533 differential responses as a whole, the vDG was the only region that alone showed statistically significant
534 responses. Together with its strong bias towards specific stimuli, as demonstrated for both theta and
535 gamma power during investigation bouts (Fig. 4B-C), these results suggest a unique and central role for
536 the vDG in orchestrating neural activity across the social brain during social behavior. This conclusion

agrees with previous studies reporting a central role of the dentate gyrus in social behavior, in general (Cai et al., 2018; Doucette et al., 2020; Leung et al., 2018), and specifically, in social discrimination (Cope et al., 2020; Li et al., 2022). Notably, multiple studies have implicated the DG in coding contextual changes. For example, DG neurons were shown to rapidly detect and encode contextual changes (Leutgeb et al., 2007), while a knockout mouse for NMDA receptors specifically in DG granule cells abolished the ability of the mutant mice to distinguish between two similar contexts (McHugh et al., 2007). Moreover, hypothalamic supramammillary neurons projecting to the DG were shown to be activated by contextual novelty (Chen et al., 2020), while the activity of ventral hippocampal neurons was shown to process information in a social context-sensitive manner (Wu et al., 2023). These studies are thus in line with our findings regarding the involvement of the vDG in dominating context-dependent social behavior.

In conclusion, our results suggest that the distribution of LFP rhythmic activity in the social brain and, most specifically, coherence between the various regions, which is dictated by the vDG, is context-specific and may thus mediate context-specific processing of social information, leading to social context-dependent social responses and behavior.

553 **Methods**

554 Animals

555 Adult male and female CD1 mice (12-14 weeks old) were acquired from Invigo (Rehovot, Israel). All mice
556 were housed in groups of 3-5 in a dark/light 12-hour cycle with *ad libitum* food and water. Following
557 surgery, implanted mice were housed in isolation so as to not disturb the implanted EAr. Experiments
558 were performed in the dark phase of the dark/light cycle in a sound- and electromagnetic noise-
559 attenuated chamber. All experiments were approved by the Institutional Animal Care and Use Committee
560 of the University of Haifa (Ethical approval #616/19).

561

562 Surgery

563 Mice were anesthetized using isoflurane (induction 3%, 0.5%-0.8% maintenance in 200mL/min of air;
564 SomnoSuite) and placed over a custom-made heating pad (37°C) in a standard stereotaxic device (Kopf
565 Instruments, Tujunga, CA). Two burr holes were drilled for placing the ground and reference wires (silver
566 wire, 127 µm, 300-500 Ω; A-M Systems, Carlsborg, WA). Two watch screws (0-80, 1/16", M1.4) were
567 inserted into the temporal bone. The coordinates for Prl (AP= 2mm, ML= -0.3, DV= -1.8), AcbC (AP= 1, ML=
568 -2.3, DV= -4.7), Pir (AP= -2, ML= -3.3, DV = -5) and CA1 (AP= -3, ML= -3.3, DV = -4.7) were indicated over
569 the left hemisphere using a marker. The skull covering these marked coordinates was removed using a
570 dental drill, and the exposed brain was kept moist with cold, sterile saline. We custom-designed the EA
571 (Mohapatra et al., 2022) from 16 individual 50 µm formvar-insulated tungsten wires (50-150 kΩ,
572 #CFW2032882; California Wire Company). Before implantation, the EAr was dipped in DiI (1,1'-
573 Dioctadecyl-3,3,3',3'-tetramethylindocarbocyanine perchlorate; 42364, Sigma-Aldrich) to visualize
574 electrode locations *post-mortem*. The reference and ground wires were inserted into their respective burr
575 holes. The EAr was lowered onto the surface of the exposed brain using a motorized manipulator (MP200;
576 Sutter instruments). The dorsoventral coordinates were marked using the depth of the electrode targeting
577 the PVN (AP= -1 mm, ML= -0.3), which was lowered slowly to -4.7 mm. The EA and exposed skull with the
578 screws were secured with dental cement (Enamel plus, Micerium). Mice were sub-cutaneously injected
579 with Baytril (5mg/kg; Bayer) and Norocarp (5 mg/kg; Carprofen, Norbrook Lab) post-surgery and allowed
580 to recover for three days.

581

582 Electrophysiological and video recordings

583 Following brief exposure to isoflurane, subjects were attached to the headstage (RHD 32 ch, #C3314, Intan
584 Technologies) through a custom-made Omnetics to Mill-Max adaptor (Mill-Max model 852-10-100-10-

585 001000). Behavior was recorded using a monochromatic camera (30 Hz, Flea3 USB3, Flir) placed above
586 the arena. Electrophysiological recordings were made with the RHD2000 evaluation system using an ultra-
587 thin SPI interface cable connected to the headstage board (RHD 16ch, #C3334, Intan Technologies).
588 Electrophysiological recordings (sampled at 20 kHz) were synchronized with recorded video using a TTL
589 trigger pulse and by recording camera frame strobes.
590
591 Experiment design
592 We recorded the behavior and neural activity of 14 males in the SP task, 13 males in the ESP task, and 11
593 males in the SxP task (Table S1), while targeting 18 distinct brain regions. All the stimuli used for the tasks
594 were unfamiliar to the subject mice. In experiments, the mice were briefly exposed to isoflurane, and the
595 EAr was connected to the evaluation system. After 10 minutes of habituation, the recordings started in
596 the arena (30 x 22 x 35 cm) with empty triangular chambers (12 cm isosceles, 35 cm height), as previously
597 described (Netser et al., 2019). The triangular chambers had one face ending with metal mesh (18 mm x
598 6 cm; 1 cm x 1 cm holes) through which the mice interacted with the stimuli. The test was divided into
599 two 5 min periods, a baseline period (pre-encounter) and a period of encounter with the stimuli. The
600 stimuli for the SP task were a novel group-housed male mouse (social) and a Lego toy (object). For the ESP
601 task, isolated (7-14 days) male and group-housed male mice served as stimuli. Finally, for the SxP task,
602 group-housed male and female mice were used as stimuli. Each subject was evaluated for three sessions
603 of each task. We excluded sessions from further evaluations when there was either removal of the
604 headstage from the EA by subjects or video recording from a session was missing, which accounts for the
605 unequal number of sessions and subjects across tasks.
606
607 Histology
608 Subjects were transcardially perfused, and their brains was kept cold in 4% paraformaldehyde for 48 h.
609 Brains were sectioned (50 µm) horizontally (VT 1200s, Leica). Electrode marks were visualized (DiI coated,
610 Red) against DAPI-stained sections with an epifluorescence microscope (Ti2 eclipse, Nikon). The marks
611 were used to locate the respective brain regions, based on the mouse atlas.
612
613 Behavioral analysis
614 Subject behavior was tracked using the TrackRodent algorithm (Netser et al., 2019) for tethered mice.
615 Further parameters of behavior, like duration of interaction, interaction bouts, distance traveled by the

subjects, subject speed, transitions between stimuli, and RDI values were calculated from the tracked results with custom codes written in MATLAB 2020a.

Electrophysiological data analysis

Only brain regions recorded for more than 5 sessions across at least 3 mice were analyzed. All signals were analyzed with codes custom-written in MATLAB 2020a. First, the signals were down-sampled to 5 kHz and low-pass filtered to 300 Hz using a Butterworth filter. The power and time for the different frequencies were estimated using the 'spectrogram' function in MATLAB with the following parameters: Discrete prolate spheroidal sequences (dpss) window = 2 s; overlap = 50% ; increments = 0.5 Hz; and time bins = 0.5 s. The power of each frequency band (theta: 4-12 Hz and gamma: 30-80 Hz) was averaged for both the baseline and encounter periods. Change in theta (ΔθP) and gamma (ΔγP) powers for each brain region were defined as the mean difference in power between the encounter and baseline periods (Fig. 2C-D, H-I). We calculated $^{\Delta}\theta P$ and $^{\Delta}\gamma P$ throughout each investigation bout for a stimulus using Z-score analysis, where the pre-bout 5 s period served as baseline. Furthermore, for each task, we averaged the Z-score across all bouts with the same stimulus in each session and compared these between the two stimuli (Fig. 8, S6 and S3). LFP power ($^{\Delta}\theta P$ and $^{\Delta}\gamma P$) for specific bouts with each stimulus was estimated by calculating the difference between the average power per second during an investigation bout (which was longer than 2 s) during the encounter period and the average power per second for investigation of both empty chambers in the baseline period of the same session, followed by averaging these values over all sessions (Fig. 4).

Coherence analysis

We used the 'mscohere' function of MATLAB to estimate coherence values using Welch's overlapped averaged periodogram method. The magnitude-squared coherence between two signals, x, and y, was defined as follows:

$$Coherence_{xy} = \frac{S_{xy}}{\sqrt{S_{xx}\, S_{yy}}}$$

where S_{xy} is the cross-power spectral density of x and y, S_{xx} is the power spectral density of x and S_{yy} is the power spectral density of y. All coherence analysis was quantified between brain regions pairs involved in at least five sessions of behavior tasks. Coherence for the baseline period was quantified as the average coherence of all brain region pairs for each context (Fig. 5A and F). Changes in coherence

(ΔθCo and ΔγCo) during the encounter period (Fig. 5B and G) between a pair of brain regions were calculated as follows:

$$Change\ in\ Coherence = \frac{\mu\ (Coherence_{encounter} - Coherence_{baseline})}{\sigma\ (Coherence_{encounter} - Coherence_{baseline})}$$

where, $Coherence_{encounter}$ is the absolute coherence value between a pair of regions within a frequency band during whole encounter period. $Coherence_{baseline}$ is the absolute coherence value between a pair of regions within a frequency band during an entire encounter period. The change in coherence for specific bouts ($^{\Delta}\theta Co$ and $^{\Delta}\gamma Co$) to each stimulus was estimated by calculating the difference between the average coherence per second during an investigation bout (≥2 s) in the encounter period and the average coherence per second for investigation with both empty chambers during the baseline period of the same session, followed by averaging these values over all sessions (Fig. 6A and S5C). Brain regions that displayed higher frequencies of crossing the threshold of mean ± 1.5 SD $^{\Delta}\theta Co$ and $^{\Delta}\gamma Co$, based on a binomial distribution test, were considered to be hubs in the coherent social brain (Fig. 7A-B).

<u>Assessing inter-regional pairwise conditional Granger causality</u>

We employed the multi-variate GC toolbox (Barnett and Seth, 2014) to calculate GC values separately for baseline and encounter periods between brain regions separately for each task and rhythm. To this end, we selected brain regions most represented among brain region pairs that crossed the mean ± 1.5*SD threshold for the difference in coherence change between preferred and less preferred stimuli in any task, separately for $^{\Delta}\theta Co$ and $^{\Delta}\gamma Co$. For GC analysis, LFP signals were measured at a reduced sampling rate of 500 Hz. We used the "tsdata_to_infocrit" function to determine the model order of the vector autoregressive (VAR) model. The median model order for all three tasks was 38 (Bayesian information criterion). To further fit the VAR model to our multi-session, multivariate LFP data, the "tsdata_to_var" function of LWR (Levinson-Whittle recursion) in the regression mode and a median model order of 38 was used separately for the baseline and encounter periods of each task. Next, we estimated the autocovariance sequence of the fitted VAR model with the "var_to_autocov" function. To maximize the computational efficiency of the function, an acmaxlags of 1500 was chosen. This process did not violate the autocovariance VAR model, as was estimated by the "var_info" function. Finally, we calculated the pairwise conditional frequency-domain multivariate GC matrix using the "autocov_to_spwcgc" function, and summed the GC for the relevant frequency band (theta or famma) using the "smvgc_to_mvgc" function.

677

678 Assessing neural responses to behavioral events

679 We divided all investigation bouts into specific behavioral events, such as the start and end of an
680 investigation bout or transition from one stimulus to the other (Fig. 7A, nine distinct types). We aligned
681 LFP power and behavior events for each stimulus by calculating mean power 5 s before and 5 s after the
682 beginning (or end) of all investigation bouts (0.5 s bins) in a session. Furthermore, for each bout, the mean
683 power was normalized using Z-score analysis, where a pre-bout duration of 5 s served as baseline (Table
684 S2).

685

686 Statistical analysis

687 Statistical analysis was performed using GraphPad Prism 9.5. To test for normal distribution of the data,
688 we used the Kolmogorov-Smirnov and Shapiro-Wilk tests. Table S3 summarizes the specific tests
689 conducted for each figure. A paired t-test or Wilcoxon matched-pairs signed rank test was used to
690 compare different stimuli or conditions for the same group. An unpaired t-test or Mann-Whitney test was
691 performed to compare a parameter between distinct groups. For comparison among multiple groups and
692 parameters, ANOVA (normal distribution), Welch's ANOVA (assuming unequal variance), and Kruskal-
693 Wallis test (non-normal distribution) were applied to the data. If a main effect or interaction were found
694 in the tests above, Šídák's test, Dunnett's T3 test or Dunn's *post-hoc* multiple comparison corrections were
695 applied. Repeated measures ANOVA or a Friedman test was used to compare multiple groups and
696 parameters with repeated variables. When main effects were observed in above tests, Šídák's or Dunn's
697 test were used for multiple comparisons corrections, respectively. Additionally, for comparison of two
698 factors and the interaction between them, from multiple groups and parameters where one of the factors
699 has repeated measurements, was performed using two-way ANOVA (no missing variables) or mixed-
700 models ANOVA (Restricted maximum likelihood model, REML). The ANOVA tests were followed by Šídák's
701 multiple comparison test if main effects or interactions were found. The association between two groups
702 or parameters was compared with either Pearson's or Spearman's tests. A binomial distribution test was
703 performed to compare the probability of brain regions representing above-chance levels for specific
704 parameters.

705

706 Decision tree classifier model

707 **Data normalization – subtracting the mean value for each brain regions pair per mouse:** The data from
708 two mice (total 14) were ignored as they had less than 40 recorded brain regions pairs (out of 99). The

mean value of each pair was computed and subtracted for each mouse separately. This helped to reduce the variability of the measurements across mice and improved classification accuracy. To reduce over-representation of a single stimulus in the computation of the mean value for a pair, we first averaged the mean value per stimulus (for a specific mouse) and then subtracted the average of these means.

Averaging bouts: The average bout for each stimulus was computed for each session.

Data Imputation: For each mouse, a slightly different set of brain areas were recorded due to slight inaccuracies in placing the electrodes and slight difference in the individual mouse anatomy. This resulted in missing entries from some of the brain regions pairs. We used a data imputation strategy to restore these missing entries. Note that before this step, we subtracted the mean value per brain region per mouse and averaged all the bouts from the same stimuli of the same session. The imputation algorithm is based on the MICE algorithm (Azur et al., 2011). It is an iterative algorithm. In each iteration, it estimates the missing entries by a linear combination of (some of) the other entries. The used data imputation algorithm was defined as follows:

1. For each missing value of brain pair i in bout b, ($bp_{i,b}$), replace $bp_{i,b}$ with the average value of bp_i across the valid values bp_i (from all bouts of all mice with a valid measurement of bp_i).
2. For each bp_i $(order\ of\ brain\ pairs\ is\ randomized)$:
    a. Randomly choose a set of predicting brain pairs $\{bp_j\}$ such that $bp_i \notin \{bp_j\}$ and $|\{bp_j\}|$ < 0.5*number_of_equations. Where the number_of_equations equals to the number of (averaged) bouts from all the mice (66 predicting brain pairs as the number of bouts in our dataset is 131 average bouts).
    b. Compute linear regression coefficients {aj} (by least square method) to minimize:

$$\underset{\{a_j\}}{\operatorname{argmin}} \sum_b \left(bp_{i,b} - \left(a_0 + \sum_j a_j bp_{j,b} \right) \right)^2$$

    c. For each bout b in which $bp_{i,b}$ was not measured in-vivo, replace it with its estimation: $a_0 + \sum_j a_j bp_{j,b}$
3. Repeat steps 2 for 20 iterations.

Code was implemented in Matlab 2021a.

Classification and computation of confusion matrixes: We used Matlab's *TreeBagger()* function to train a multi-class Random forest classifier for discriminating between a pair of stimuli (social vs object) or

contexts (3 classes) or between stimuli (6 classes) or between. We used 80 random trees (a parameter of the TreeBagger function). We used cross-validation with "one mouse leave out" strategy to compute a confusion matrix for each mouse based on a training set that includes examples from all of the other mice. We balanced the training set to have the same number of examples from each class by randomly removing some of the training examples. Since both the balancing and the Random forest algorithm have a random component, we repeated the estimation of confusion matrixes 100 times (for each mouse) to better estimate the confusion matrixes. We then summed up all of the confusion matrixes (totally 1200 confusion matrixes: 12 mice and 100 confusion matrixes per mouse) and computed for each pair of classes (i,j) the percent of cases where the prediction was i for bouts of class j.

Statistical Analysis: To compute p-values, we used the average (over 100 iterations) confusion matrix for each mouse (totally 12 confusion matrixes in which each cell i,j represents the % of predictions of class i for bouts of class j) and compare those with a set of random confusion matrixes which were generated by the same procedure except for replacing the trained classifier with a random classifier. This random classifier generated random labels with uniform distribution. To better describe the distribution of the random confusion matrixes, we generated 83 random confusion matrixes per mouse (each one of them is an average of 100 confusion matrixes). Then, the p-value for each cell in the confusion matrix was computed separately by comparing the 12 values from the confusion matrix of the trained classifier to the 83*12=996 values from the confusion matrixes of the random classifier using Mann-Whitney U test. In case a mouse did not have a bout from a specific class, this mouse was ignored in the computation of the p-value for the cells of this ground truth class.

Declarations

Acknowledgments

We thank Boris Shklyar, Head of the Bio-imaging Unit and Dr. Maya Lalzar, Head of the Bioinformatics Unit of the Faculty of Natural Sciences of the University of Haifa for their guidance and technical assistance. We also thank Eng. Alex Bizer, the experimental systems engineer of the Faculty of Natural Sciences of the University of Haifa, for their help.

Funding:

This study was supported by ISF-NSFC joint research program (grant No. 3459/20 to SW), the Israel Science Foundation (grants No. 1361/17 and 2220/22 to SW), the Ministry of Science, Technology and

Space of Israel (Grant No. 3-12068 to SW) and the United States-Israel Binational Science Foundation (grant No. 2019186 to SW).

Author contributions

A.N.M.: Formal analysis, Investigation, Methodology, Validation, Visualization, Writing - original draft, and Writing - review & editing; D.P.: Formal analysis, and software.; S.N.: Data curation, Project administration, Software, Validation, Visualization, Writing - original draft, and Writing - review & editing. S.W.: Conceptualization, Funding acquisition, Project administration, Resources, Supervision, Writing - original draft, and Writing - review & editing.

Declaration of interests

The authors declare no competing interests.

782 **Supplementary figures**

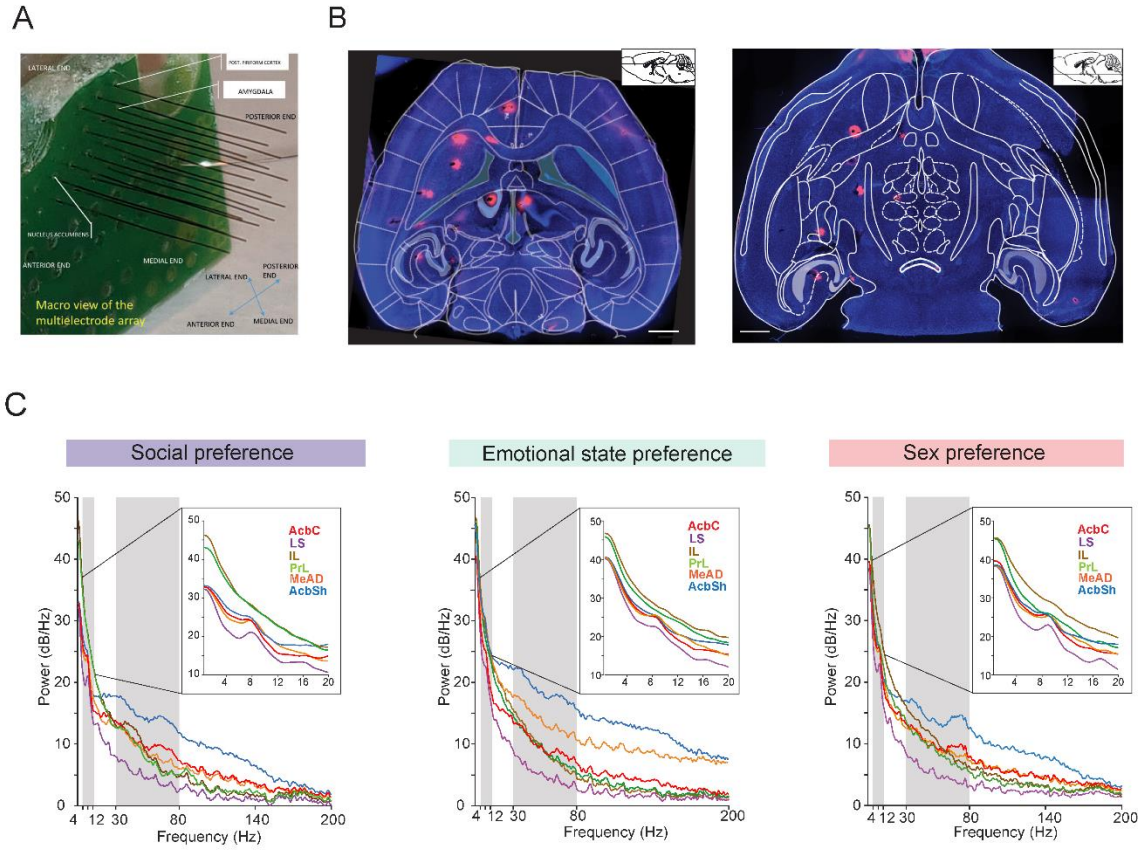

783

784 **Figure S1: The electrode array and PSD profiles from individual sessions**

785 A. Macro-view of the electrode array

786 B. Brain sections from mice with DiI-mediated electrode tip marks (red) in the targeted regions overlaid
787 on an atlas image of a similar DV plane. Left section = -2.36 mm from Bregma, right section = -4.72
788 mm, scale = 1 mm

789 C. The power spectral density (PSD) plots of LFP signals recorded in the MeAD, IL, PrL, CA1, AcbC, and
790 AcbSh during the encounter period of SP (left), EsP (middle) and SxP (right) task single sessions, all
791 conducted by the same mouse. The inset shows the PSD plots for 0-20 Hz band at higher resolution.

792

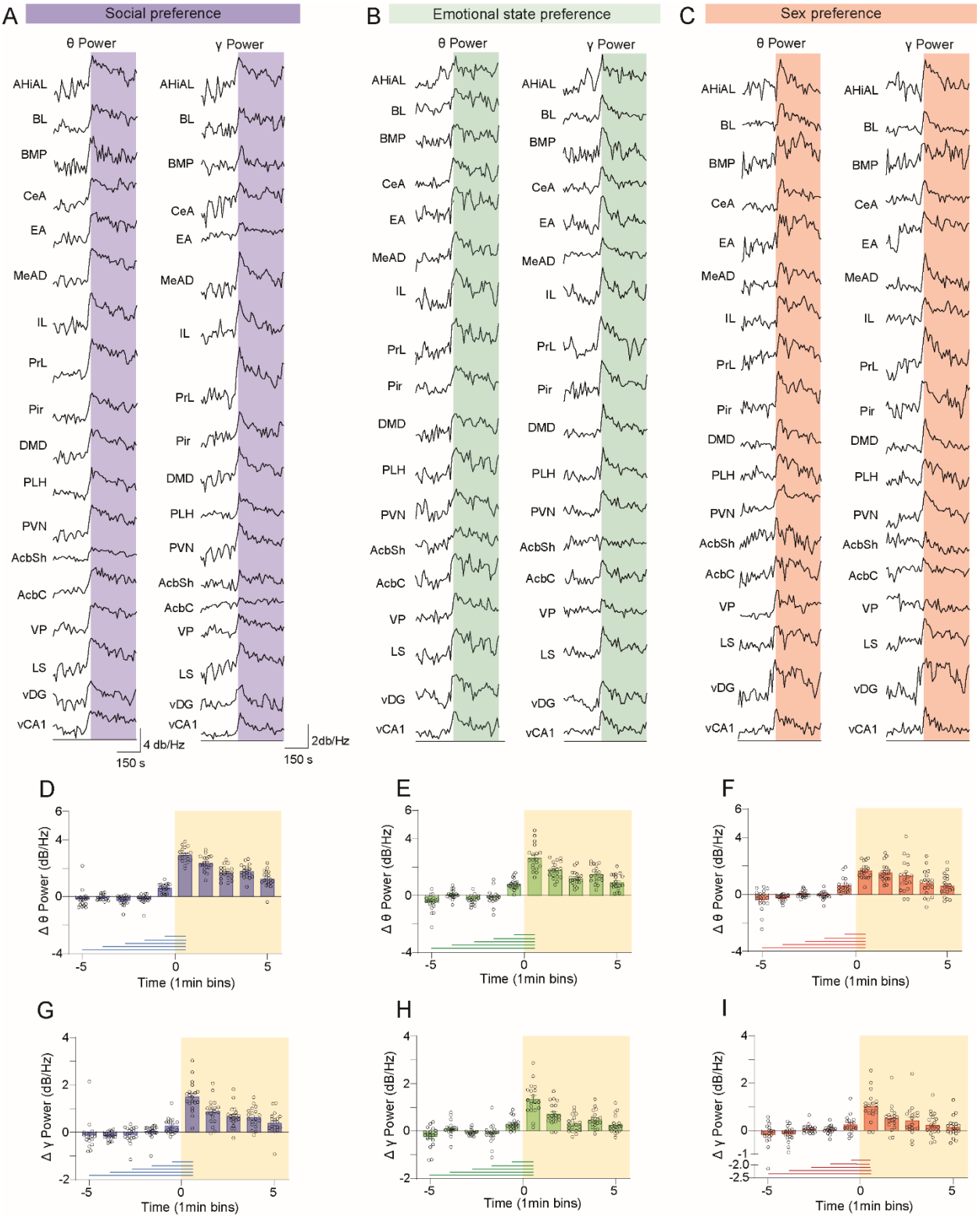

Figure S2. Similar dynamics of theta and gamma power across the various tasks and brain regions

A. Mean traces of ΔθP (left column) and ΔγP (right column) across all sessions of the SP task for each brain region. The colored bar represents the encounter period.

B. As in A, for the EsP task

C. As in A, for the SxP task

D. Mean (±SEM) ΔθP, averaged across all brain regions for every minute of the baseline and encounters periods of the SP task. Time 0 min represents the time of stimuli insertion. Lines below the bars represent a significant difference between the first minute of the encounter and every minute of the baseline period.

E. As in D, for the EsP task.

F. As in D, for the SxP task

G-I, as in D-F, for ΔγP.

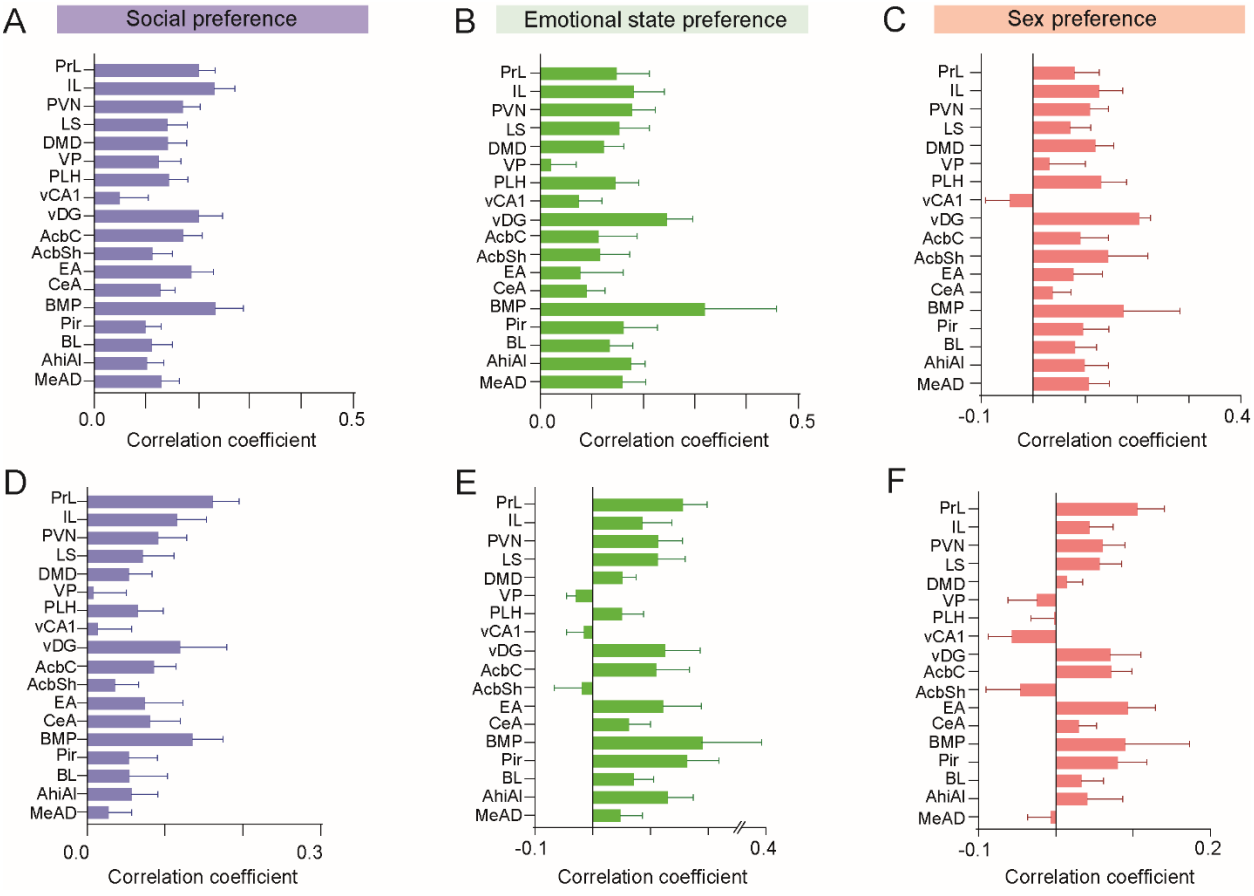

Figure S3. No correlation exists between theta and gamma power changes during social encounters and subject speed

A. Correlation coefficients across all SP task sessions for calculating Pearson's correlation between the change in theta power (ΔθP) and the mean speed of the subject.

B. As in A, for EsP sessions.

C. As in A, for SxP sessions.

D-F. As in A-C, for gamma power (ΔγP).

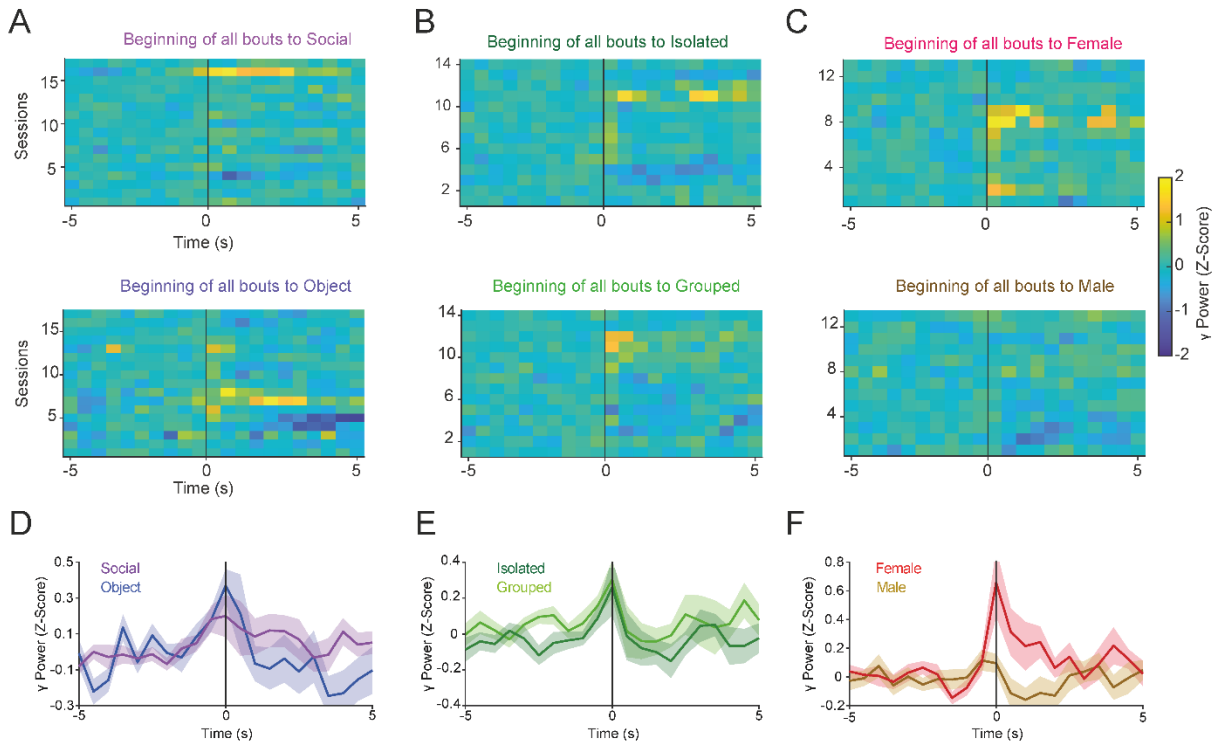

Figure S4. Z-score analysis of changes in gamma power during social investigation of specific stimuli

A. Heat maps of average gamma power in AhiAl, before and during social investigation bouts of subjects with social (above) and object (below) stimuli. Each row represents the mean Z-score of all bouts in a single session (using 0.5 s bins). Time '0' represents the beginning of the bout. The color code scale is on the right.

B. As in A, for investigation bouts of isolated (above) and grouped (below) social stimuli during EsP tasks.

C. As in A, for investigation bouts of female (above) and male (below) social stimuli during SxP tasks.

D. Mean (±SEM) Z-score trace of the data shown in A for both stimuli.

E. As in D. for the data shown in B.

F. As in D, for the data shown in C.

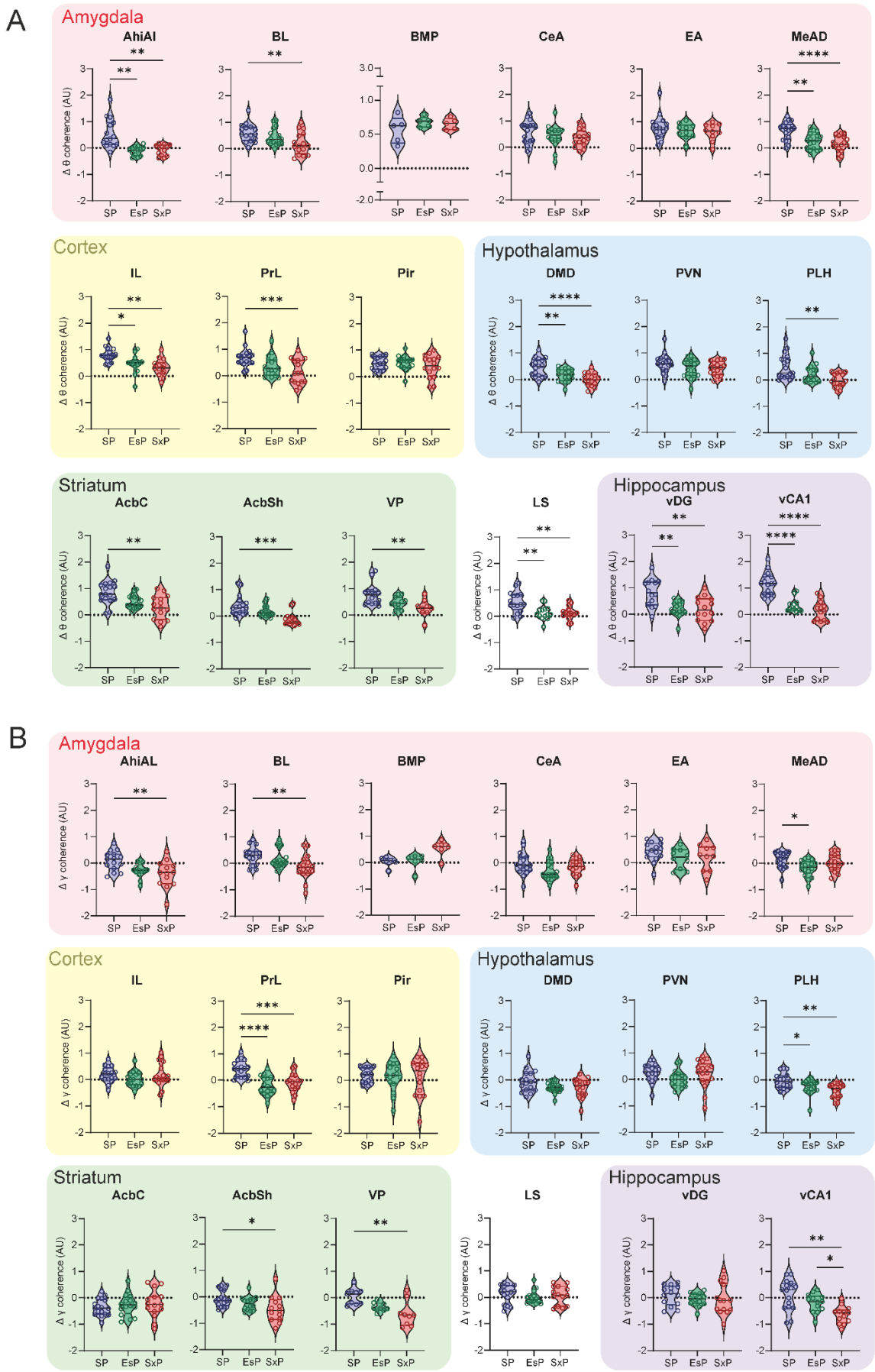
A
Amygdala
AhiAl
BL
BMP
CeA
EA
MeAD
Cortex
IL
PrL
Pir
Hypothalamus
DMD
PVN
PLH
Striatum
AcbC
AcbSh
VP
LS
Hippocampus
vDG
vCA1
Δ θ coherence (AU)
SP
EsP
SxP
B
Amygdala
AhiAL
BL
BMP
CeA
EA
MeAD
Cortex
IL
PrL
Pir
Hypothalamus
DMD
PVN
PLH
Striatum
AcbC
AcbSh
VP
LS
Hippocampus
vDG
vCA1
Δ γ coherence (AU)
SP
EsP
SxP

Figure S5. Coherence changes during the encounter period of the various tasks are brain region-specific

A. Mean change in theta coherence (ΔθCo) between a given brain region and all other simultaneously recorded regions during the encounter period, compared across the three tasks.

B. As in A, for gamma coherence (ΔγCo).

*p<0.05, **p<0.01, ***p<0.001, ****p<0.0001, Dunnett's and Dunn's *post-hoc* test following the main effect in ANOVA and Kruskal Wallis test, respectively.

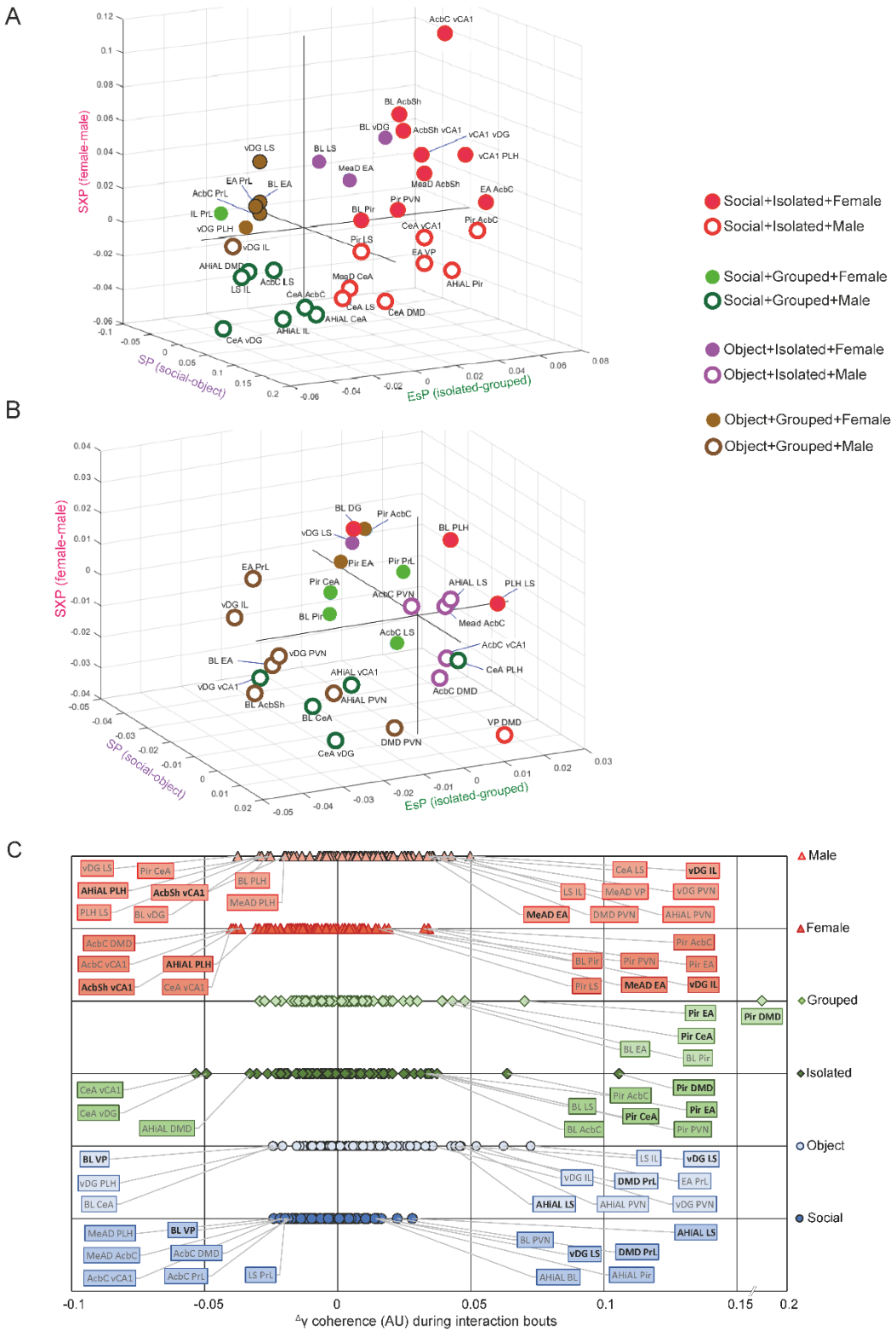
A
SXP (female-male)
SP (social-object)
EsP (isolated-grouped)
AcbC vCA1
BL AcbSh
BL vDG
AcbSh vCA1
vCA1 vDG
vCA1 PLH
vDG LS
BL LS
MeaD EA
MeaD AcbSh
EA AcbC
EA PrL
BL EA
AcbC PrL
IL PrL
vDG PLH
BL Pir
Pir PVN
Pir AcbC
CeA vCA1
Pir LS
EA VP
vDG IL
AHiAL DMD
AcbC LS
LS IL
MeaD CeA
AHiAL Pir
CeA AcbC
CeA LS
CeA DMD
AHiAL CeA
AHiAL IL
CeA vDG
B
SXP (female-male)
SP (social-object)
EsP (isolated-grouped)
BL DG
Pir AcbC
vDG LS
BL PLH
Pir EA
Pir PrL
EA PrL
Pir CeA
AHiAL LS
PLH LS
AcbC PVN
vDG IL
BL Pir
Mead AcbC
AcbC LS
AcbC vCA1
vDG PVN
BL EA
CeA PLH
AHiAL vCA1
vDG vCA1
AcbC DMD
BL AcbSh
AHiAL PVN
BL CeA
VP DMD
DMD PVN
CeA vDG
Social+Isolated+Female
Social+Isolated+Male
Social+Grouped+Female
Social+Grouped+Male
Object+Isolated+Female
Object+Isolated+Male
Object+Grouped+Female
Object+Grouped+Male
C
Male
Female
Grouped
Isolated
Object
Social
vDG LS
Pir CeA
AHiAL PLH
AcbSh vCA1
BL PLH
MeAD PLH
PLH LS
BL vDG
CeA LS
vDG IL
LS IL
MeAD VP
vDG PVN
MeAD EA
DMD PVN
AHiAL PVN
AcbC DMD
AcbC vCA1
AHiAL PLH
AcbSh vCA1
CeA vCA1
BL Pir
Pir PVN
Pir AcbC
Pir EA
Pir LS
MeAD EA
vDG IL
Pir EA
Pir DMD
Pir CeA
BL EA
BL Pir
CeA vCA1
CeA vDG
AHiAL DMD
Pir AcbC
Pir DMD
BL LS
Pir EA
Pir CeA
BL AcbC
Pir PVN
BL VP
vDG PLH
BL CeA
LS IL
vDG LS
vDG IL
DMD PrL
EA PrL
AHiAL LS
AHiAL PVN
vDG PVN
MeAD PLH
BL VP
MeAD AcbC
AcbC DMD
AcbC vCA1
AcbC PrL
LS PrL
BL PVN
vDG LS
DMD PrL
AHiAL LS
AHiAL BL
AHiAL Pir
-0.1
-0.05
0
0.05
0.1
0.15
0.2
Δγ coherence (AU) during interaction bouts

836

837 **Figure S6. Distribution of theta and gamma coherence changes during social investigation bouts across**
838 **tasks**

839 A. A 3D representation of the mean difference in theta coherence change during investigation bouts
840 ($^{\Delta}\theta Co$) between the preferred and less-preferred stimuli, across all tasks. Each dot represents a pair
841 of brain regions (n = 84 pairs), color- and shape-coded according to the combined bias across all tasks.
842 Only pairs which showed a coherence change of 1.5*SD from the mean are presented. We excluded
843 any pair with fewer than five sessions of investigation bouts with one of the stimuli or with both.

844 B. As in A, for gamma coherence change ($^{\Delta}\gamma Co$)

845 C. Distribution of gamma coherence change ($^{\Delta}\gamma Co$) between each pair of brain regions during
846 investigation bouts, plotted separately for each stimulus used in the SP (blue), EsP (green) and SxP
847 (red) tasks. The brain region pairs which passed the mean ± 1.5*SD cutoff are labeled and those that
848 are shared by both stimuli in the same task are denoted in bold.

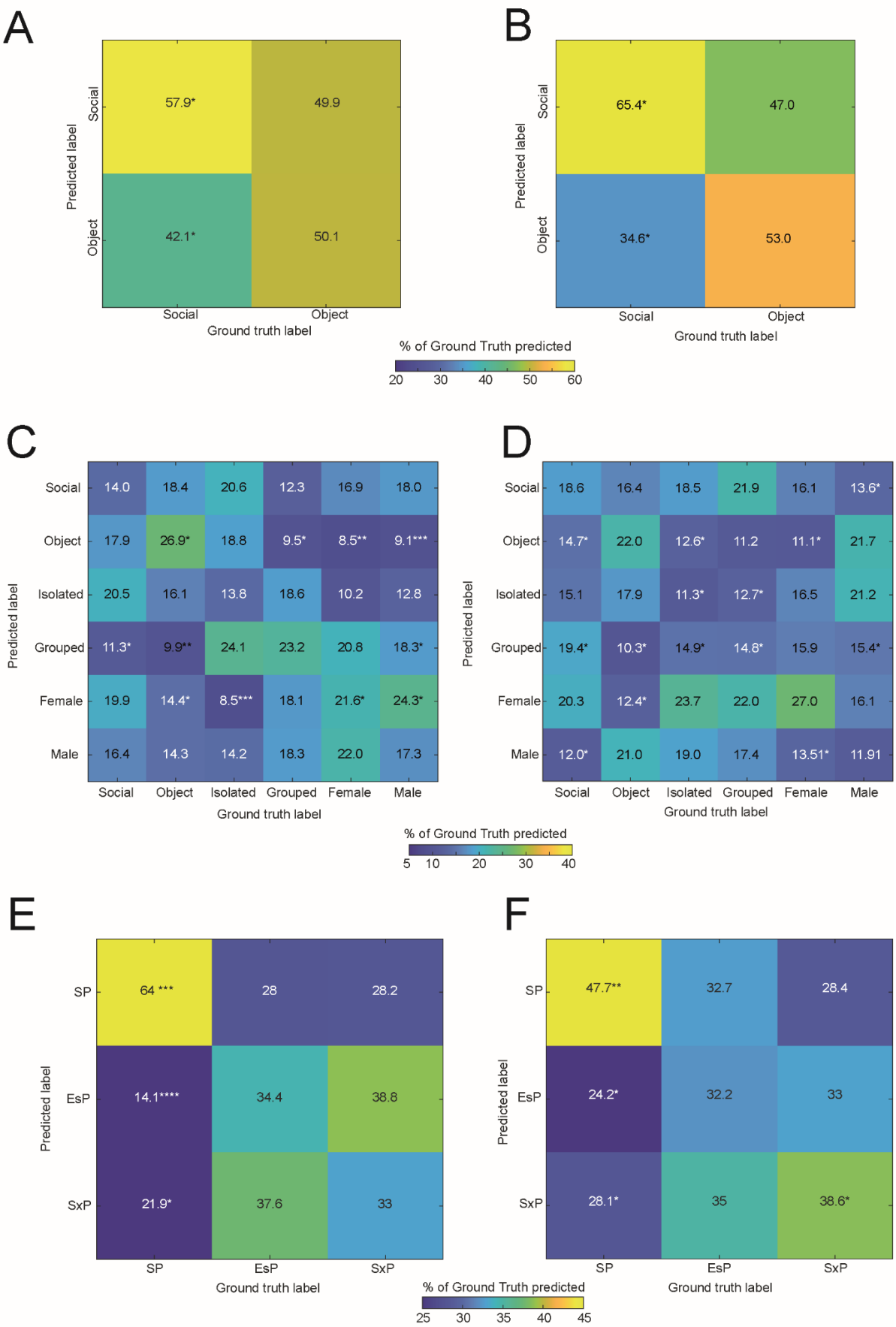
A
Predicted label
Social
Object
57.9*
49.9
42.1*
50.1
Social
Object
Ground truth label
B
Predicted label
Social
Object
65.4*
47.0
34.6*
53.0
Social
Object
Ground truth label
% of Ground Truth predicted
20 30 40 50 60
C
Predicted label
Social 14.0 18.4 20.6 12.3 16.9 18.0
Object 17.9 26.9* 18.8 9.5* 8.5** 9.1***
Isolated 20.5 16.1 13.8 18.6 10.2 12.8
Grouped 11.3* 9.9** 24.1 23.2 20.8 18.3*
Female 19.9 14.4* 8.5*** 18.1 21.6* 24.3*
Male 16.4 14.3 14.2 18.3 22.0 17.3
Social Object Isolated Grouped Female Male
Ground truth label
D
Predicted label
Social 18.6 16.4 18.5 21.9 16.1 13.6*
Object 14.7* 22.0 12.6* 11.2 11.1* 21.7
Isolated 15.1 17.9 11.3* 12.7* 16.5 21.2
Grouped 19.4* 10.3* 14.9* 14.8* 15.9 15.4*
Female 20.3 12.4* 23.7 22.0 27.0 16.1
Male 12.0* 21.0 19.0 17.4 13.51* 11.91
Social Object Isolated Grouped Female Male
Ground truth label
% of Ground Truth predicted
5 10 20 30 40
E
Predicted label
SP 64 *** 28 28.2
EsP 14.1**** 34.4 38.8
SxP 21.9* 37.6 33
SP EsP SxP
Ground truth label
F
Predicted label
SP 47.7** 32.7 28.4
EsP 24.2* 32.2 33
SxP 28.1* 35 38.6*
SP EsP SxP
Ground truth label
% of Ground Truth predicted
25 30 35 40 45

849

Figure S7. Random forest model can predict the social stimulus in the SP task but not the specific stimulus among all six stimuli

A. A color-coded confusion matrix of a multi-class Random Forest classifier using the changes in theta coherence during investigation bouts across the SP task to predict the type of investigated stimulus among the two possible stimuli (social and object).
B. As in A, for gamma coherence.
C. A color-coded confusion matrix of the same model using the changes in theta coherence during investigation bouts across all tasks to predict the type of investigated stimulus among the six possible stimuli.
D. As in C, for gamma coherence.
E. A color-coded confusion matrix for the Random Forest classifier employed for predicting the social context from $^{\Delta}\theta P$ values across all brain regions and stimuli. The scale of the accuracy's color code is shown to the right. The percentage of cases a label was predicted for each ground truth are marked in the middle of each spot. *p<0.05, **<0.01, ***<0.001, ****<0.0001, Mann-Whitney test.
F. As in E, for the combination of $^{\Delta}\theta P$ and $^{\Delta}\theta Co$. *p<0.05, **<0.01, Mann-Whitney test.

867

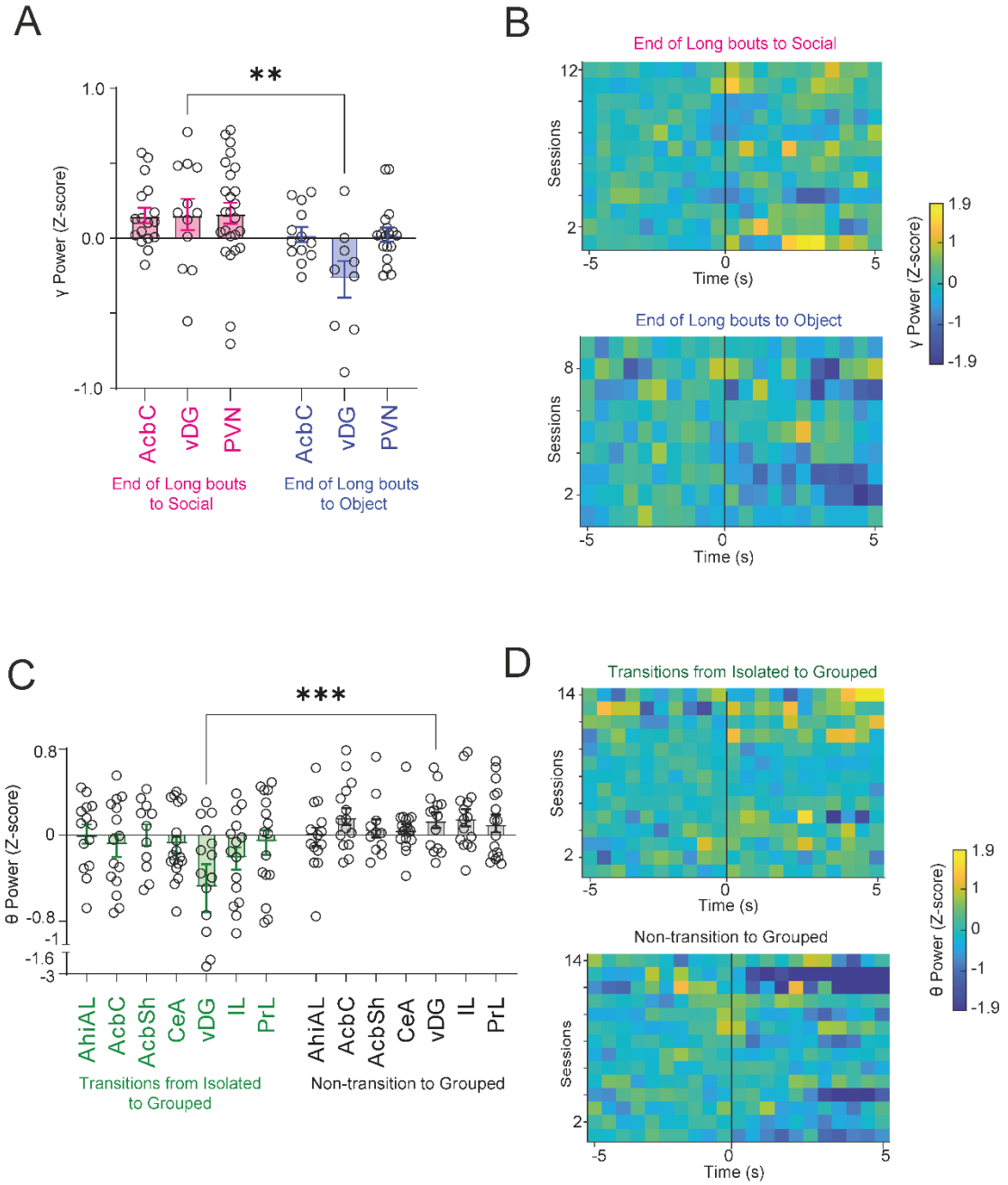

868

869 **Figure S8. Significant difference in gamma and theta power in specific behavioral events**

870 A. Mean (±SEM) Z-score values of gamma power change in the vDG at the end of long (>3 s) investigation
871 bouts towards social (pink) and object (blue) stimuli during SP task sessions, shown for three brain
872 regions where significant changes in GC were found in the gamma band.

B. Heat maps of male vDG gamma power changes before and during long (>3 s) investigation bouts towards the social (above) and object (below) stimuli across all SP task sessions. Each row represents the mean Z-score of all bouts in a single session (bins of 0.5s). Time point **'0'** represents the beginning of the bout. The color code is on the r

C-D. As in A-B, for changes in theta power at the beginning of transitional vs. non-transitional investigation bouts of grouped social stimuli across EsP sessions.

References

Adolphs, R. (2010). Conceptual challenges and directions for social neuroscience. Neuron 65, 752-767.

Azur, M.J., Stuart, E.A., Frangakis, C., and Leaf, P.J. (2011). Multiple imputation by chained equations: what is it and how does it work? Int J Methods Psychiatr Res 20, 40-49.

Barnett, L., and Seth, A.K. (2014). The MVGC multivariate Granger causality toolbox: a new approach to Granger-causal inference. J Neurosci Methods 223, 50-68.

Benchenane, K., Tiesinga, P.H., and Battaglia, F.P. (2011). Oscillations in the prefrontal cortex: a gateway to memory and attention. Curr Opin Neurobiol 21, 475-485.

Bocchio, M., Nabavi, S., and Capogna, M. (2017). Synaptic Plasticity, Engrams, and Network Oscillations in Amygdala Circuits for Storage and Retrieval of Emotional Memories. Neuron 94, 731-743.

Buzsaki, G., and Draguhn, A. (2004). Neuronal oscillations in cortical networks. Science 304, 1926-1929.

Buzsaki, G., and Wang, X.J. (2012). Mechanisms of gamma oscillations. Annu Rev Neurosci 35, 203-225.

Buzsaki, G., and Watson, B.O. (2012). Brain rhythms and neural syntax: implications for efficient coding of cognitive content and neuropsychiatric disease. Dialogues Clin Neurosci 14, 345-367.

Cai, Y., Tang, X., Chen, X., Li, X., Wang, Y., Bao, X., Wang, L., Sun, D., Zhao, J., Xing, Y.*, et al.* (2018). Liver X receptor beta regulates the development of the dentate gyrus and autistic-like behavior in the mouse. Proc Natl Acad Sci U S A 115, E2725-E2733.

Cannon, J., McCarthy, M.M., Lee, S., Lee, J., Borgers, C., Whittington, M.A., and Kopell, N. (2014). Neurosystems: brain rhythms and cognitive processing. Eur J Neurosci 39, 705-719.

Chen, S., He, L., Huang, A.J.Y., Boehringer, R., Robert, V., Wintzer, M.E., Polygalov, D., Weitemier, A.Z., Tao, Y., Gu, M.*, et al.* (2020). A hypothalamic novelty signal modulates hippocampal memory. Nature 586, 270-274.

Chen, S., Tan, Z., Xia, W., Gomes, C.A., Zhang, X., Zhou, W., Liang, S., Axmacher, N., and Wang, L. (2021). Theta oscillations synchronize human medial prefrontal cortex and amygdala during fear learning. Sci Adv 7.

Clayton, M.S., Yeung, N., and Kadosh, R.C. (2015). The roles of cortical oscillations in sustained attention. Trends in Cognitive Sciences 19, 188-195.

Colgin, L.L. (2011). Oscillations and hippocampal-prefrontal synchrony. Curr Opin Neurobiol 21, 467-474.

Cope, E.C., Waters, R.C., Diethorn, E.J., Pagliai, K.A., Dias, C.G., Tsuda, M., Cameron, H.A., and Gould, E. (2020). Adult-Born Neurons in the Hippocampus Are Essential for Social Memory Maintenance. Eneuro 7.

912 Dai, B., Sun, F., Tong, X., Ding, Y., Kuang, A., Osakada, T., Li, Y., and Lin, D. (2022). Responses and
913 functions of dopamine in nucleus accumbens core during social behaviors. Cell Rep 40, 111246.
914 Dickinson, S.Y., Kelly, D.A., Padilla, S.L., and Bergan, J.F. (2022). From Reductionism Toward Integration:
915 Understanding How Social Behavior Emerges From Integrated Circuits. Front Integr Neurosci 16,
916 862437.
917 Dolen, G., Darvishzadeh, A., Huang, K.W., and Malenka, R.C. (2013). Social reward requires coordinated
918 activity of nucleus accumbens oxytocin and serotonin. Nature 501, 179-184.
919 Doucette, E., Merfeld, E., Leblanc, H., Monasterio, A., Cincotta, C., Grella, S.L., Logan, J., and Ramirez, S.
920 (2020). Social behavior in mice following chronic optogenetic stimulation of hippocampal engrams.
921 Neurobiol Learn Mem 176, 107321.
922 Felix-Ortiz, A.C., Burgos-Robles, A., Bhagat, N.D., Leppla, C.A., and Tye, K.M. (2016). Bidirectional
923 modulation of anxiety-related and social behaviors by amygdala projections to the medial prefrontal
924 cortex. Neuroscience 321, 197-209.
925 Felix-Ortiz, A.C., and Tye, K.M. (2014). Amygdala inputs to the ventral hippocampus bidirectionally
926 modulate social behavior. J Neurosci 34, 586-595.
927 Fiebelkorn, I.C., and Kastner, S. (2019). A Rhythmic Theory of Attention. Trends in Cognitive Sciences 23,
928 87-101.
929 Ford, C.L., and Young, L.J. (2021). Translational opportunities for circuit-based social neuroscience:
930 advancing 21st century psychiatry. Curr Opin Neurobiol 68, 1-8.
931 Fries, P. (2015). Rhythms for Cognition: Communication through Coherence. Neuron 88, 220-235.
932 Geschwind, D.H., and Levitt, P. (2007). Autism spectrum disorders: developmental disconnection
933 syndromes. Curr Opin Neurobiol 17, 103-111.
934 Goodson, J.L. (2005). The vertebrate social behavior network: evolutionary themes and variations. Horm
935 Behav 48, 11-22.
936 Gordon, J.A. (2011). Oscillations and hippocampal-prefrontal synchrony. Curr Opin Neurobiol 21, 486-
937 491.
938 Harris, A.Z., and Gordon, J.A. (2015a). Long-range neural synchrony in behavior. Annu Rev Neurosci 38,
939 171-194.
940 Harris, A.Z., and Gordon, J.A. (2015b). Long-Range Neural Synchrony in Behavior. Annual Review of
941 Neuroscience, Vol 38 38, 171-194.
942 Headley, D.B., and Pare, D. (2013). In sync: gamma oscillations and emotional memory. Front Behav
943 Neurosci 7, 170.

944 Helfrich, R.F., Breska, A., and Knight, R.T. (2019). Neural entrainment and network resonance in support
945 of top-down guided attention. Curr Opin Psychol 29, 82-89.
946 Huang, W.C., Zucca, A., Levy, J., and Page, D.T. (2020). Social Behavior Is Modulated by Valence-Encoding
947 mPFC-Amygdala Sub-circuitry. Cell Rep 32, 107899.
948 Insel, T.R., and Fernald, R.D. (2004). How the brain processes social information: searching for the social
949 brain. Annu Rev Neurosci 27, 697-722.
950 Jabarin, R., Levy, N., Abergel, Y., Berman, J.H., Zag, A., Netser, S., Levy, A.P., and Wagner, S. (2021).
951 Pharmacological modulation of AMPA receptors rescues specific impairments in social behavior
952 associated with the A350V Iqsec2 mutation. Transl Psychiatry 11, 234.
953 John, S.R., Dagash, W., Mohapatra, A.N., Netser, S., and Wagner, S. (2022). Distinct Dynamics of Theta
954 and Gamma Rhythmicity during Social Interaction Suggest Differential Mode of Action in the Medial
955 Amygdala of Sprague Dawley Rats and C57BL/6J Mice. Neuroscience 493, 69-80.
956 Karakas, S. (2020). A review of theta oscillation and its functional correlates. Int J Psychophysiol 157, 82-
957 99.
958 Kingsbury, L., Huang, S., Raam, T., Ye, L.S., Wei, D., Hu, R.K., Ye, L., and Hong, W. (2020). Cortical
959 Representations of Conspecific Sex Shape Social Behavior. Neuron 107, 941-953 e947.
960 Knyazev, G.G. (2007). Motivation, emotion, and their inhibitory control mirrored in brain oscillations.
961 Neurosci Biobehav R 31, 377-395.
962 Kohl, J., Babayan, B.M., Rubinstein, N.D., Autry, A.E., Marin-Rodriguez, B., Kapoor, V., Miyamishi, K.,
963 Zweifel, L.S., Luo, L., Uchida, N., and Dulac, C. (2018). Functional circuit architecture underlying
964 parental behaviour. Nature 556, 326-331.
965 Kohl, J., and Dulac, C. (2018). Neural control of parental behaviors. Curr Opin Neurobiol 49, 116-122.
966 Kuga, N., Abe, R., Takano, K., Ikegaya, Y., and Sasaki, T. (2022). Prefrontal-amygdalar oscillations related
967 to social behavior in mice. Elife 11.
968 Lazaro, M.T., Taxidis, J., Shuman, T., Bachmutsky, I., Ikrar, T., Santos, R., Marcello, G.M., Mylavarapu, A.,
969 Chandra, S., Foreman, A.*, et al.* (2019). Reduced Prefrontal Synaptic Connectivity and Disturbed
970 Oscillatory Population Dynamics in the CNTNAP2 Model of Autism. Cell Rep 27, 2567-2578 e2566.
971 Leroy, F., Park, J., Asok, A., Brann, D.H., Meira, T., Boyle, L.M., Buss, E.W., Kandel, E.R., and Siegelbaum,
972 S.A. (2018). A circuit from hippocampal CA2 to lateral septum disinhibits social aggression. Nature
973 564, 213-218.

974 Leung, C., Cao, F., Nguyen, R., Joshi, K., Aqrabawi, A.J., Xia, S., Cortez, M.A., Snead, O.C., 3rd, Kim, J.C.,
975 and Jia, Z. (2018). Activation of Entorhinal Cortical Projections to the Dentate Gyrus Underlies Social
976 Memory Retrieval. Cell Rep 23, 2379-2391.
977 Leutgeb, J.K., Leutgeb, S., Moser, M.B., and Moser, E.I. (2007). Pattern separation in the dentate gyrus
978 and CA3 of the hippocampus. Science 315, 961-966.
979 Li, J., Sun, X., You, Y., Li, Q., Wei, C., Zhao, L., Sun, M., Meng, H., Zhang, T., Yue, W.*, et al.* (2022). Auts2
980 deletion involves in DG hypoplasia and social recognition deficit: The developmental and neural
981 circuit mechanisms. Sci Adv 8, eabk1238.
982 Mague, S.D., Talbot, A., Blount, C., Walder-Christensen, K.K., Duffney, L.J., Adamson, E., Bey, A.L.,
983 Ndubuizu, N., Thomas, G.E., Hughes, D.N.*, et al.* (2022). Brain-wide electrical dynamics encode
984 individual appetitive social behavior. Neuron 110, 1728-1741 e1727.
985 McHugh, T.J., Jones, M.W., Quinn, J.J., Balthasar, N., Coppari, R., Elmquist, J.K., Lowell, B.B., Fanselow,
986 M.S., Wilson, M.A., and Tonegawa, S. (2007). Dentate gyrus NMDA receptors mediate rapid pattern
987 separation in the hippocampal network. Science 317, 94-99.
988 McKinsey, G., Ahmed, O.M., and Shah, N.M. (2018). Neural control of sexually dimorphic social
989 behaviors. Curr Opin Physiol 6, 89-95.
990 Mohapatra, A.N., Netser, S., and Wagner, S. (2022). Modular Electrode Array for Multi-site Extracellular
991 Recordings from Brains of Freely Moving Rodents. Curr Protoc 2, e399.
992 Netser, S., Haskal, S., Magalnik, H., Bizer, A., and Wagner, S. (2019). A System for Tracking the Dynamics
993 of Social Preference Behavior in Small Rodents. J Vis Exp.
994 Netser, S., Meyer, A., Magalnik, H., Zylbertal, A., de la Zerda, S.H., Briller, M., Bizer, A., Grinevich, V., and
995 Wagner, S. (2020). Distinct dynamics of social motivation drive differential social behavior in
996 laboratory rat and mouse strains. Nat Commun 11, 5908.
997 Palva, J.M., and Palva, S. (2018). Functional integration across oscillation frequencies by cross-frequency
998 phase synchronization. Eur J Neurosci 48, 2399-2406.
999 Reis, F.M., Lee, J.Y., Maesta-Pereira, S., Schuette, P.J., Chakerian, M., Liu, J., La-Vu, M.Q., Tobias, B.C.,
1000 Ikebara, J.M., Kihara, A.H.*, et al.* (2021). Dorsal periaqueductal gray ensembles represent approach
1001 and avoidance states. Elife 10.
1002 Schaich Borg, J., Srivastava, S., Lin, L., Heffner, J., Dunson, D., Dzirasa, K., and de Lecea, L. (2017). Rat
1003 intersubjective decisions are encoded by frequency-specific oscillatory contexts. Brain Behav 7,
1004 e00710.

1005 Scheggia, D., La Greca, F., Maltese, F., Chiacchierini, G., Italia, M., Molent, C., Bernardi, F., Coccia, G.,
1006 Carrano, N., Zianni, E.*, et al.* (2022). Reciprocal cortico-amygdala connections regulate prosocial and
1007 selfish choices in mice. Nat Neurosci 25, 1505-1518.
1008 Swanson, L.W., Hahn, J.D., and Sporns, O. (2020). Structure-function subsystem models of female and
1009 male forebrain networks integrating cognition, affect, behavior, and bodily functions. Proc Natl Acad
1010 Sci U S A 117, 31470-31481.
1011 Taub, A.H., Perets, R., Kahana, E., and Paz, R. (2018). Oscillations Synchronize Amygdala-to-Prefrontal
1012 Primate Circuits during Aversive Learning. Neuron 97, 291-298 e293.
1013 Tendler, A., and Wagner, S. (2015). Different types of theta rhythmicity are induced by social and fearful
1014 stimuli in a network associated with social memory. Elife 4.
1015 Twining, R.C., Vantrease, J.E., Love, S., Padival, M., and Rosenkranz, J.A. (2017). An intra-amygdala circuit
1016 specifically regulates social fear learning. Nat Neurosci 20, 459-469.
1017 Uhlhaas, P.J., Pipa, G., Lima, B., Melloni, L., Neuenschwander, S., Nikolic, D., and Singer, W. (2009).
1018 Neural synchrony in cortical networks: history, concept and current status. Front Integr Neurosci 3,
1019 17.
1020 Uhlhaas, P.J., Roux, F., Rodriguez, E., Rotarska-Jagiela, A., and Singer, W. (2010). Neural synchrony and
1021 the development of cortical networks. Trends Cogn Sci 14, 72-80.
1022 Wei, D., Talwar, V., and Lin, D. (2021). Neural circuits of social behaviors: Innate yet flexible. Neuron 109,
1023 1600-1620.
1024 Wu, W.Y., Yiu, E., Ophir, A.G., and Smith, D.M. (2023). Effects of social context manipulation on dorsal
1025 and ventral hippocampal neuronal responses. Hippocampus.
1026 Yamamoto, R., Ahmed, N., Ito, T., Gungor, N.Z., and Pare, D. (2018). Optogenetic Study of Anterior BNST
1027 and Basomedial Amygdala Projections to the Ventromedial Hypothalamus. Eneuro 5.

1028

1029